Chapter 6

Numerical Results and Discussion

In this chapter, the new numerical results of this thesis are presented. In section 6.1 we start with numerical investigations of the relativistic electron capture process by calculations performed in various frames of reference. The influence of the number of bound-state basis functions on the total capture cross section is studied. In sections 6.2 and 6.3 parametric dependencies of electron capture on the collision energy and the charge numbers of the colliding nuclei are investigated. In sections 6.4 and 6.5 the effect of different reference frames and of Coulomb boundary conditions is elucidated systematically by numerical examples. In section 6.6 we turn to the process of bound-free pair creation in heavy-ion collisions and investigate two-centre effects. The last section 6.7 briefly describes the influence of free-particle basis functions on electron capture cross sections.

Many of the results exclusively consider electron capture. The reason is that the corresponding numerical calculations are computationally much less demanding, compared to calculations employing free-particle basis functions. Furthermore, the results presented here concerning electron capture have not been reported previously in the literature. Many computations required considerable computing time and have been performed on clusters of workstations and personal computers, and on massively parallel processor systems.

6.1 Charge transfer

In this section, charge transfer calculations are presented, which have been done with a set of basis functions only comprising bound-state wave functions. The emphasis is on the total charge-transfer cross section $\sigma_{\text{capture}}(1\text{s}_{1/2})$ for an initial electronic configuration $1\text{s}_{1/2}$. This cross section is obtained by a weighted integral over the impact-parameter-dependent transfer probability $P(b)$, where b denotes the impact parameter [EM95]:

$$\sigma_{\text{capture}}(1\text{s}_{1/2}) = 2\pi \int_0^\infty P(b) b \, \mathrm{d}b.$$

Here $P(b)$ is the sum over the approximate transition probabilities for all transitions from an initial $1\text{s}_{1/2}$-configuration of the target nucleus, to an *arbitrary* final configuration that corresponds to a bound state of the projectile nucleus. Note that the role of the target nucleus may be taken by either nucleus A or nucleus B, depending on which nucleus the initial configuration is associated with. Therefore, $P(b)$ is the sum over the probabilities of transitions to the bound states of either nucleus B or nucleus A.

Coupled channel calculations, presented in this section, have been done for three different basis sets, which respectively comprise the two, ten and 28 lowest bound states of each centre. The charge numbers of both centres are throughout $Z_\text{A}, Z_\text{B} =$

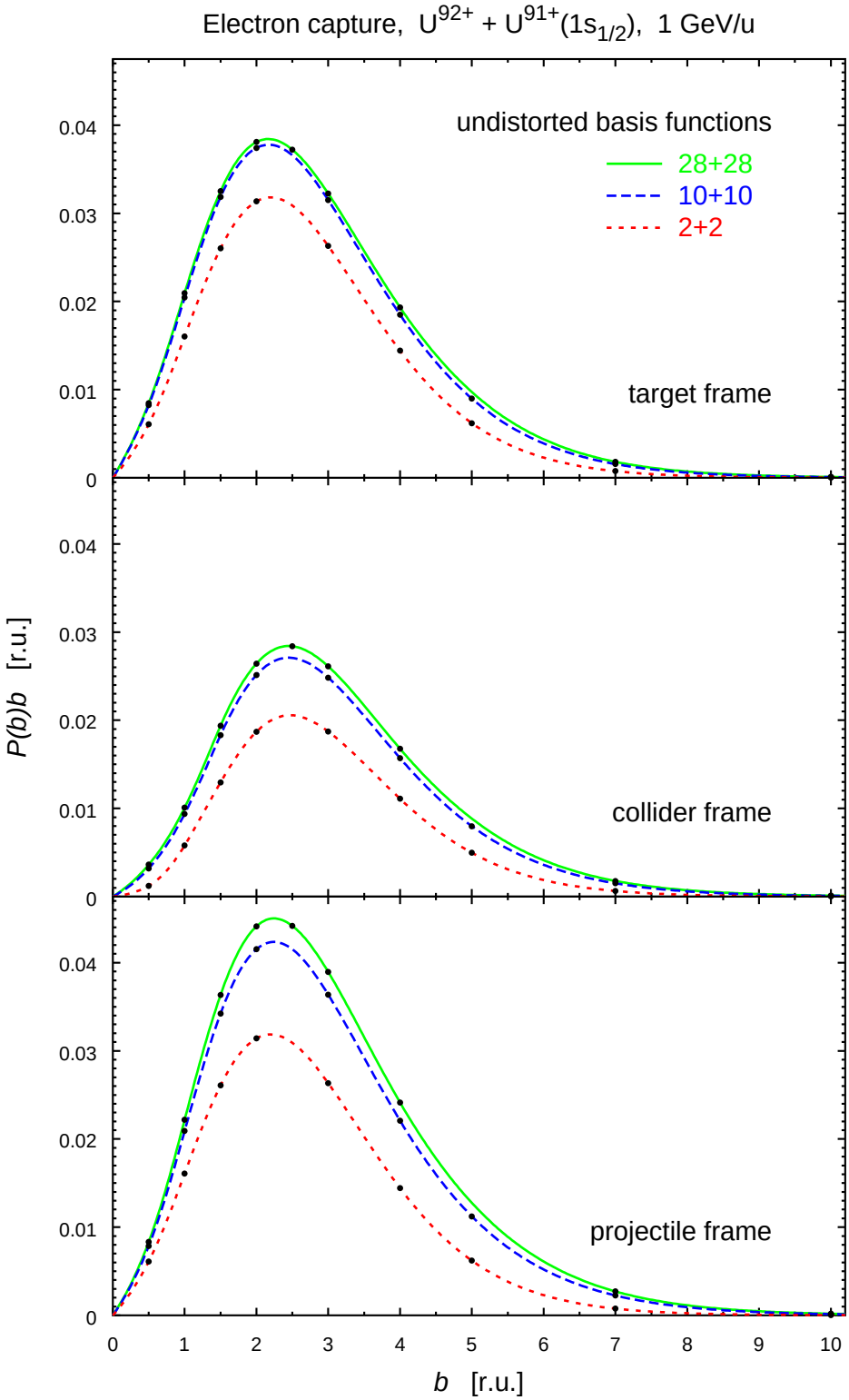

FIGURE 6.1. Weighted total capture probabilities $P(b)b$ from coupled channel calculations with *undistorted* basis functions. The initial configuration is $1s_{1/2}$ and the basis' comprise either the two, ten or 28 lowest bound states of each nucleus.

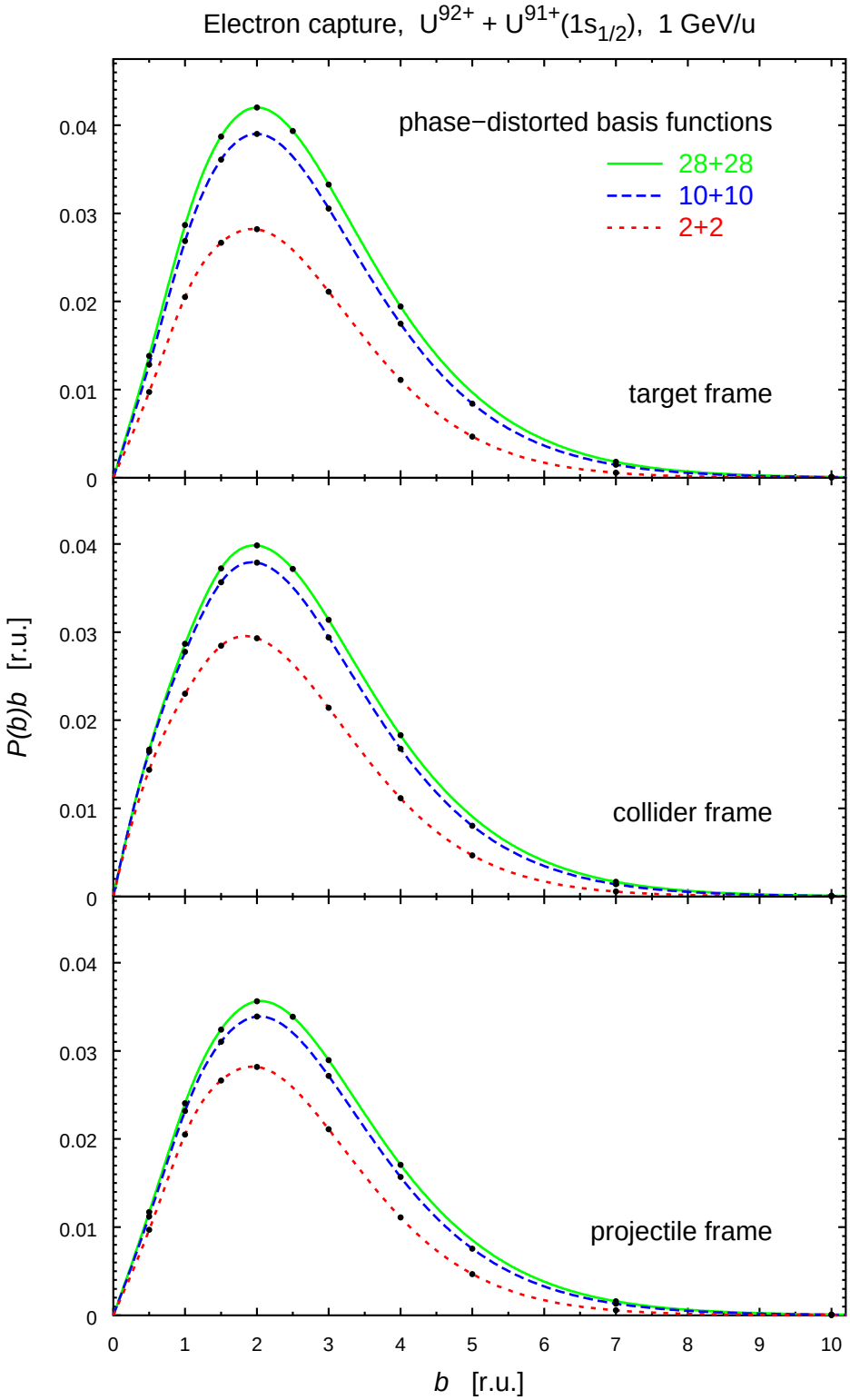

FIGURE 6.2. Weighted total capture probabilities $P(b)b$ as in figure 6.1, but obtained from coupled channel calculations with *phase-distorted* basis functions (see equation (5.12)).

TABLE 6.1. Total capture cross sections $\sigma_{\text{capture}}(1s_{1/2})$ in kbarn for the collision system $U^{91+}(1s_{1/2}) + U^{92+}$ at a collision energy of $T = 1\,\text{GeV/u}$. The first row and column of the table describe the coupled channel basis. The second row gives the frame of reference in which the coupled channel equations have been solved.

	undistorted basis			phase-distorted basis		
no. states	target	collider	projectile	target	collider	projectile
$2+2$	0.922	0.582	0.923	0.837	0.892	0.836
$10+10$	1.164	0.838	1.330	1.219	1.208	1.072
$28+28$	1.206	0.898	1.441	1.333	1.288	1.146

92, corresponding to uranium nuclei, and the collision energy is $T = 1\,\text{GeV/u}$, or equivalently $\gamma = 2.0735$. Calculations have been carried out, on one hand in the rest frame of nucleus A, and on the other hand in the collider frame, where both centres move with equal, but opposite, velocities. The calculations in the rest frame of nucleus A provide capture probabilities both for the target frame and the projectile frame, since the fundamental solution of the coupled channel equations has always been determined (cf. chapters 4 and 5). Hence, capture cross sections are obtained by a numerical solution of the coupled channel equations in the target, collider and projectile frames. These frames are illustrated in figure 1.2 on page 9.

Figure 6.1 shows the weighted capture probabilities $P(b)b$ for the calculations with undistorted basis functions. Analogous calculations, with a phase-distorted basis, are presented in the subsequent figure 6.2. The total capture cross sections are listed in table 6.1.

Discussion. Charge transfer cross sections, calculated in different Lorentz frames by means of relativistic coupled channel calculations, are presented here for the first time. The differences between charge transfer probabilities, which are obtained in different frames of reference, clearly show the violation of the Lorentz boost invariance, as a consequence of the coupled channel approximation. The cross sections computed in the *target* frame are in good agreement with similar existing data [TE90, table I][EM95, p. 241].

The simple 4-state calculations yield cross sections, which are remarkably close to the values obtained with more basis functions. This demonstrates the importance of the $1s_{1/2}$-states of the projectile for the charge transfer process [EM95]. Moreover, the differences between the cross sections, obtained with 10+10 and 28+28 basis functions, are generally smaller than the differences between the cross sections computed in different reference frames, using the same number of basis functions. Therefore, it must be expected that a further increase of the number of *bound* states, used in the coupled channel expansion, will not modify the numerical results significantly. By contrast, the difference between the results obtained in relatively moving reference frames is expected to remain, if only the number of *bound* states is increased.

The increase of the total cross section with the number of basis functions has a simple explanation: the total capture probability $P(b)$, which is plotted here, comprises the transition probabilities to an increased number of final configurations. The

small difference between the total capture cross sections obtained from calculations with 10+10 and 28+28 bound states reflects the fact that the higher bound states of the projectile are less important for the capture process. In fact, the individual transition probabilities from an initial 1s-configuration to some particular final configuration are slightly changing as well, if different sets of basis functions are used. But this represents a minor effect.

There are two conclusions from the above observations. First, a coupled channel expansion using only bound states is not a sufficient approximation to the exact solution of the two-centre Dirac equation. This fact is only revealed by the frame dependence of the results. An assessment, e.g., of the top plot of figure 6.1 alone might suggest that the coupled channel calculation has converged, in the sense that an increased number of basis functions will not modify the results. The extension of the coupled channel basis by free-particle wave functions seems to be necessary, in order to construct a better approximation to the exact solution of the two-centre Dirac equation. A more accurate approximation to this solution is then expected to provide Lorentz-frame invariance of the numerical calculations. This reflects the importance of the ionisation process for the collision system and collision energy, which have been considered. This is known from perturbation theories and is also observed in experiments [BGF+97].

Second, for a theoretical study of the capture process, using a pure bound-state basis, it is helpful to determine the cross sections in various frames of reference and thereby to obtain an estimate of the systematic error, due to the frame dependence of the calculations.

Finally, the difference between calculations with undistorted and phase-distorted basis functions should be noted: The difference between the results obtained in different Lorentz frames is smaller for calculations with phase-distorted basis functions. This suggests that the frame dependence of the capture calculations is reduced by using phase-distorted basis functions (for a more detailed discussion see section 6.4 below).

6.2 Collision-energy dependence of capture

In spite of the difficulties, regarding the frame dependence of capture calculations, it is tempting to study, by means of the coupled channel method, the parametric dependencies of the capture cross sections on the collision energy and the charge numbers of the colliding nuclei. Such a nonperturbative investigation has not been done previously. In this section results for the collision-energy dependence are presented.

Capture cross sections have been determined for different collision energies ranging from 0.4 GeV/u up to 1.3 GeV/u. Two different collision systems, $U^{91+}(1s_{1/2}) + U^{92+}$ and $Au^{78+}(1s_{1/2}) + Au^{79+}$, have been considered in three different reference frames, namely the target, collider and projectile frames (as in the previous section). Coupled channel calculations have been done, which employ the ten lowest bound states of each nucleus. The results for the total capture cross sections obtained from these

TABLE 6.2. Total capture cross sections $\sigma_{\text{capture}}(1s_{1/2})$ in units of kbarn as a function of the collision energy T for the collision system $U^{91+}(1s_{1/2}) + U^{92+}$. The cross sections have been obtained by means of coupled channel calculations using the ten lowest bound states of each nucleus.

$Z_A, Z_B = 92$	undistorted basis			phase-distorted basis		
T [GeV/u]	target	collider	projectile	target	collider	projectile
0.4	9.50	8.84	10.1	10.3	10.2	9.89
0.7	2.77	2.28	3.07	3.00	2.98	2.75
1.0	1.16	0.838	1.33	1.22	1.21	1.07
1.4	0.618	0.384	0.711	0.606	0.599	0.516

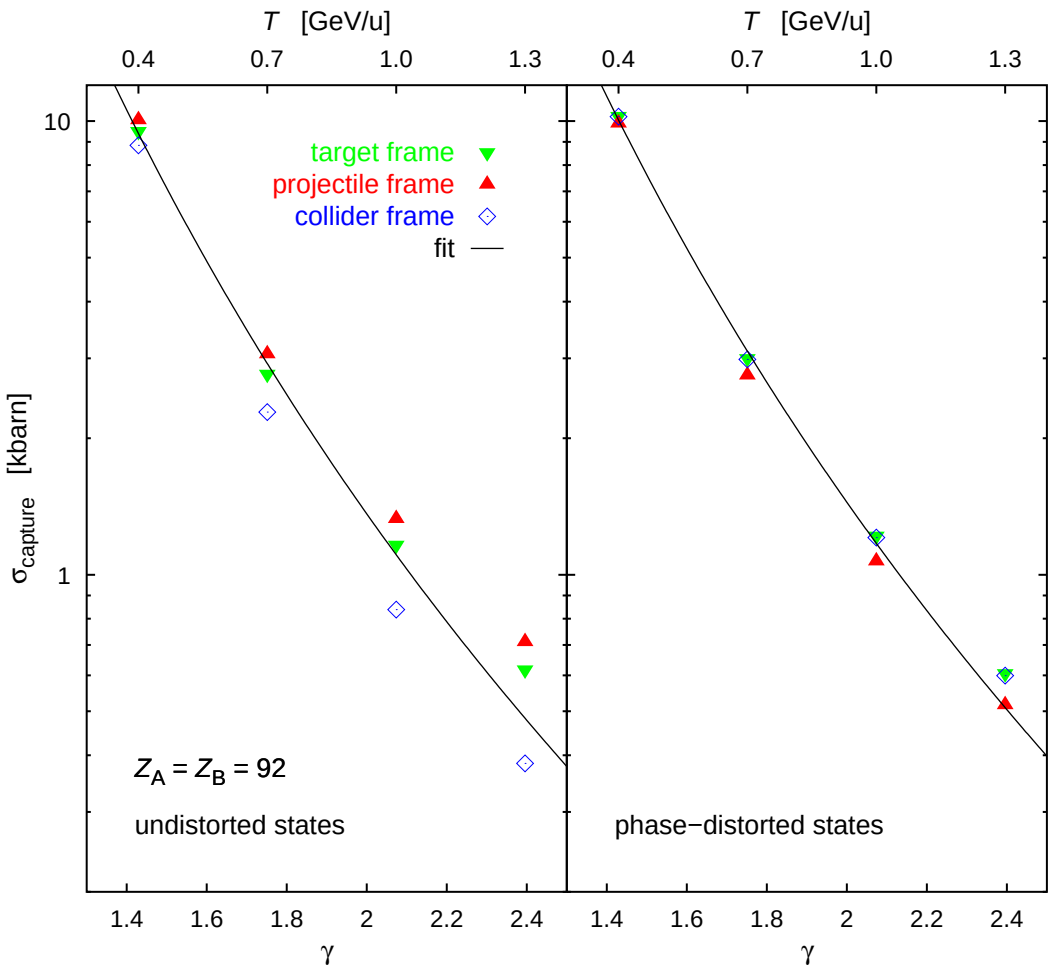

FIGURE 6.3. Collision-energy dependence of electron capture by a bare uranium projectile from hydrogen-like uranium with an initial 1s-configuration. The cross sections plotted here correspond to the numerical values given in table 6.2.

TABLE 6.3. Total capture cross sections in units of kbarn as in table 6.2, but for the collision system $Au^{78+}(1s_{1/2}) + Au^{79+}$.

$Z_A, Z_B = 79$	undistorted basis			phase-distorted basis		
T [GeV/u]	target	collider	projectile	target	collider	projectile
0.4	7.35	6.96	7.73	7.47	7.51	7.11
0.7	1.84	1.55	1.98	1.75	1.76	1.58
0.96	0.812	0.606	0.868	0.703	0.707	0.610
1.4	0.376	0.237	0.393	0.281	0.287	0.237

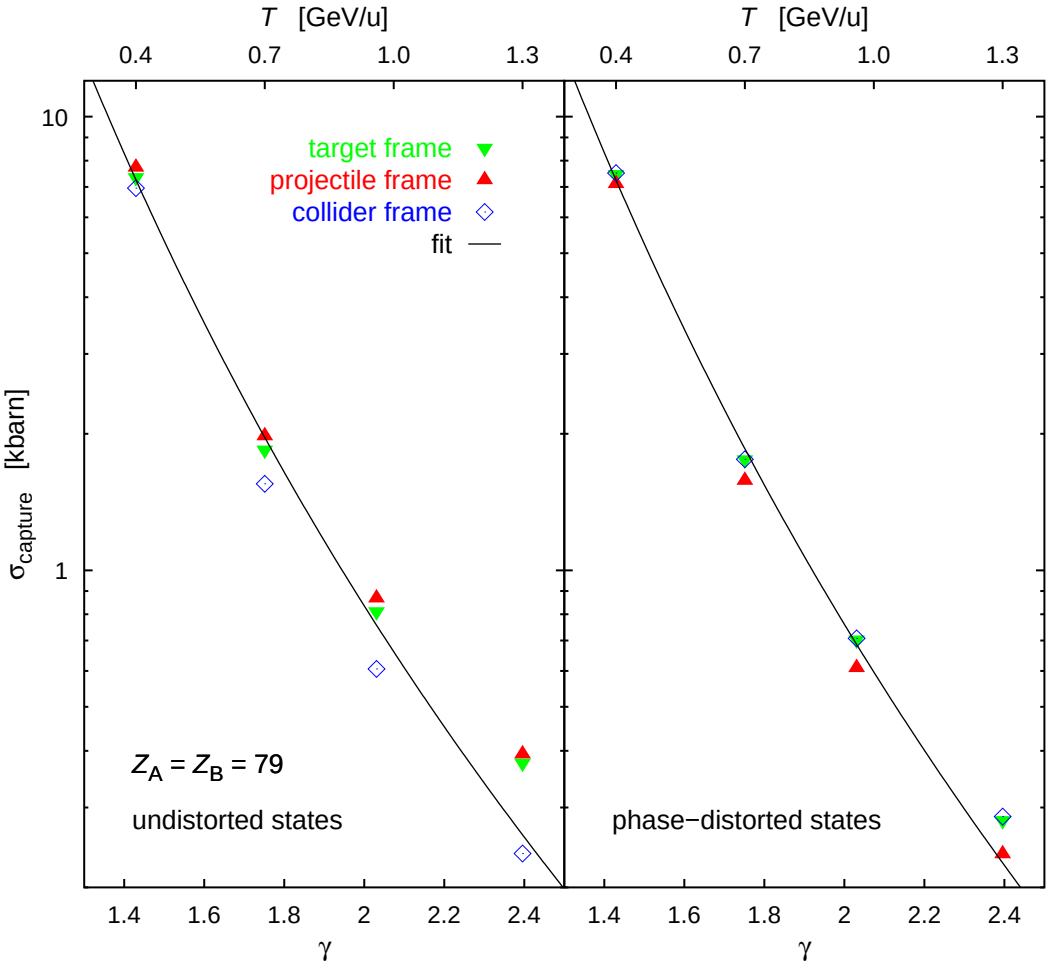

FIGURE 6.4. As figure 6.3, but for hydrogen-like gold colliding with a bare gold projectile. The cross sections plotted here correspond to the numerical values given in table 6.3.

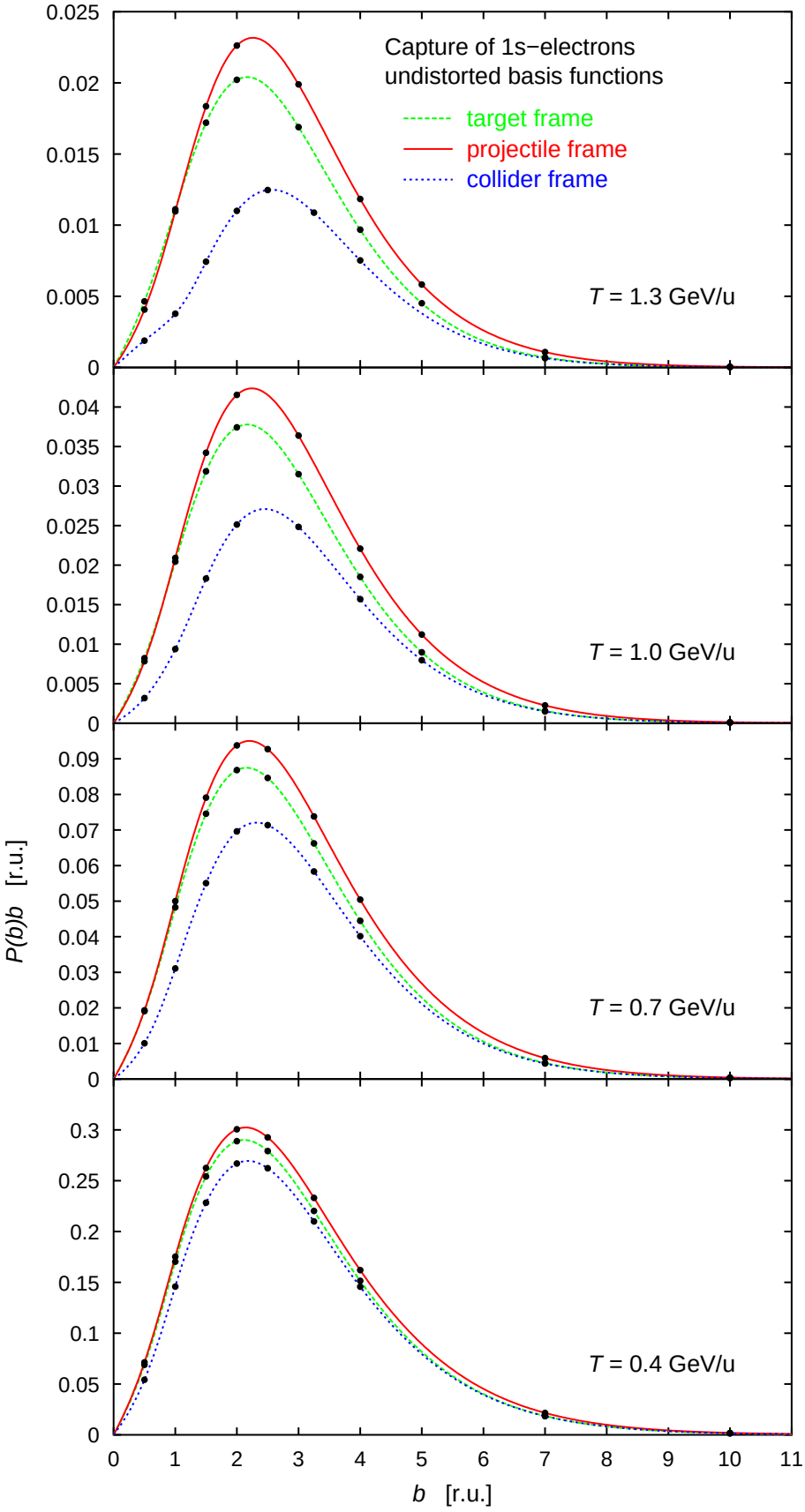

FIGURE 6.5. Weighted total capture probabilities $P(b)b$ as a function of the impact parameter b for the collision system $U^{91+}(1s_{1/2})+U^{92+}$. The results shown here have been obtained by calculations with an undistorted basis. Regarding the length scale, note that the K-shell radius of uranium is 1.5 r.u..

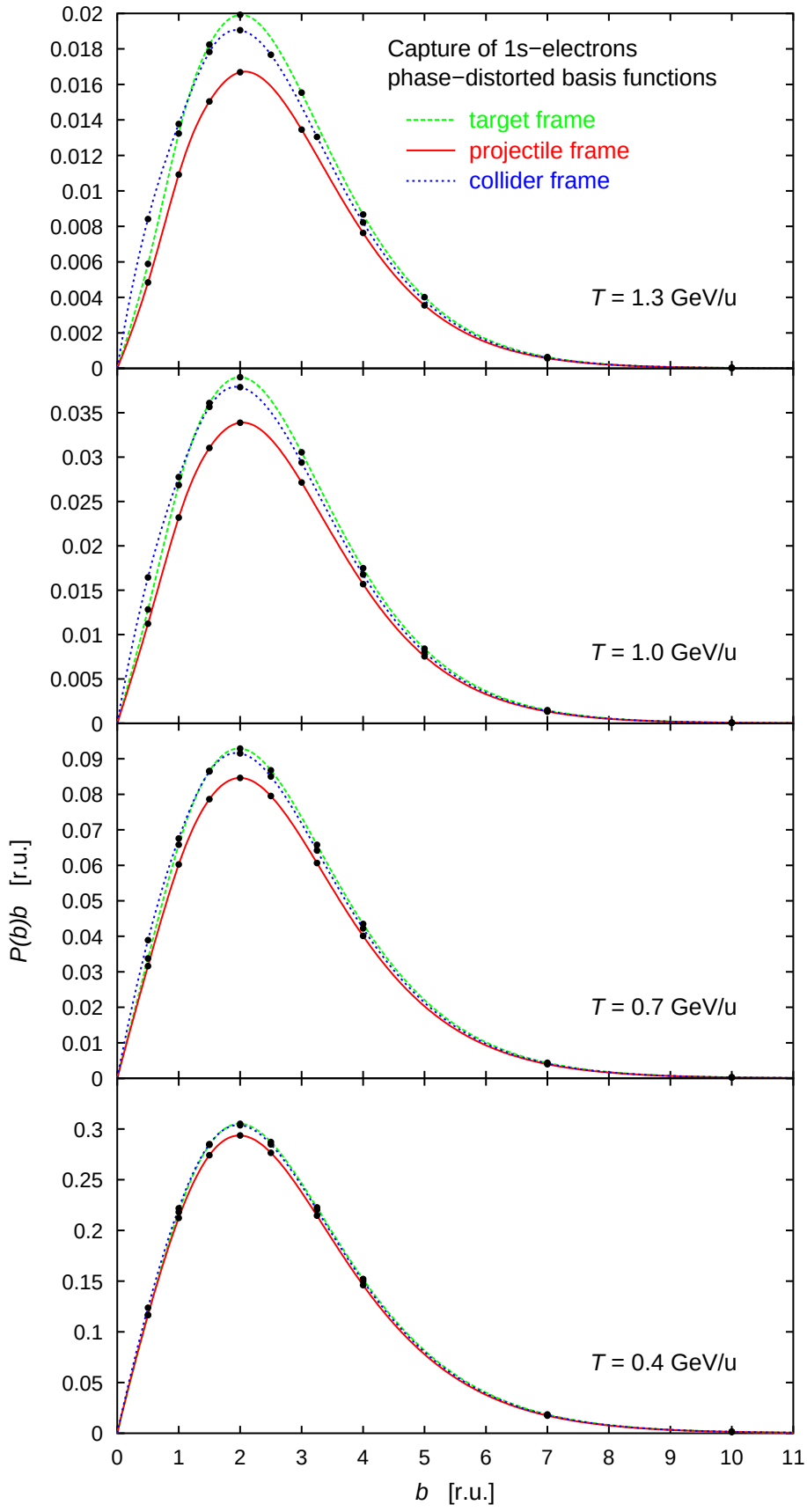

FIGURE 6.6. The same as in figure 6.5, but corresponding to calculations with a phase-distorted basis functions.

calculations are given in the tables 6.2 and 6.3. The same data is presented in the figures 6.3 and 6.4.

In both figures, a fit to the energy dependence of the total capture cross section is shown as well. For the determination of the fit functions, the mean values of the capture cross sections obtained in different reference frames have been fitted to the function,

$$\sigma_{\text{capture}}(1\text{s}_{1/2}) = a\gamma^{-b}, \tag{6.1}$$

by a numerical least-squares algorithm. Here again, γ denotes the Lorentz factor describing the collision energy (cf. section 2.1). The values for the fit parameters a and b are given in table 6.4, for both collision systems and calculations with undistorted as well as phase-distorted basis functions. In this table also alternative fit functions are presented, which are of the form $\sigma_{\text{capture}}(1\text{s}_{1/2}) = aT^{-b}$, where T is the kinetic energy of the collision given in GeV/u.

Finally, the figures 6.5 and 6.6 show the weighted total capture probabilities $P(b)b$ as a function of the impact parameter b, but for the symmetrical uranium collision system only.

Discussion. A principal feature, exhibited by the figures 6.3 and 6.4, is the remarkably similar energy dependence obtained from calculations with undistorted and phase-distorted basis functions. Furthermore, the absolute values of the total cross sections are comparable for both methods of calculation. This relationship is very different compared to the corresponding perturbative capture theories. Note that the coupled channel calculations with undistorted basis functions as well as the perturbative Oppenheimer–Brinkmann–Kramers (OBK) approximation [EM95] correspond to a scattering theory not taking into account the long-range character of the Coulomb interaction. On the other hand calculations with phase-distorted basis functions as well as the boundary-corrected Born approximation (B1B) [EM95] are approximations to the exact scattering theory with Coulomb boundary conditions. In the literature, it has been found that generally the simple OBK cross sections are significantly larger than the B1B cross sections and that the latter provide a better description of experimentally measured cross sections of (nonradiative) electron capture [EM95]. Such a difference is not observable for the presumably more accurate coupled channel approaches presented here.

As observed already in the previous section, the difference of the cross sections from calculations in different reference frames is clearly smaller, if a phase-distorted basis is used. As demonstrated in particular by the figures 6.5 and 6.6, the frame dependence of the cross sections increases for growing collision energy. This reflects the fact that a Lorentz boost between the rest frames of both centres mixes time and spatial coordinates more weakly as the collision energy decreases (leading to the Galilean transform in the limit of very small collision energies).

For the range of collision energies chosen here, various perturbation theories are available for a comparison with the present results [EM95]. Almost all of these perturbative approximations predict a dependence of the capture cross section which is proportional to γ^{-1} for large collision energies. More precisely, the relativistic unsymmetrical eikonal theory of electron capture [Eic85, ISE93, EM95], which provides

TABLE 6.4. Fit parameters for the collision-energy dependence of the capture cross sections, given in table 6.2 and 6.3. The arithmetic mean values of cross sections obtained in different reference frame have been fitted to the respective functions given in the first row, using a least-squares fit. Here, γ denotes the Lorentz factor giving the collision energy and T denotes the kinetic energy in GeV/u.

	fit function	$\sigma[\text{kbarn}] = a\gamma^{-b}$		$\sigma[\text{kbarn}] = aT^{-b}$	
Z_A, Z_B		a	b	a	b
92 (U)	undist. basis	73	5.7	1.1	2.3
	ph.-dist. basis	79	5.8	1.2	2.4
79 (Au)	undist. basis	72	6.4	0.69	2.6
	ph.-dist. basis	80	6.7	0.60	2.8

satisfactory agreement with many experiments, shows such a decrease of the cross section for collision energies above 10 GeV/u. The collision energy dependence, as predicted by nonrelativistic capture theories for high collision velocities, is T^{-6} in first-order and $T^{-5.5}$ in second order perturbation theory [BM92]. Therefore, the fits to the present relativistic coupled channel results, given in table 6.4, show that the range of collision energies around 1 GeV/u constitutes an intermediate region, between the high energy regimes of nonrelativistic and relativistic perturbative capture theories. The presently found much faster decrease of the capture cross section, as compared to the relativistic high energy behaviour, is also predicted by the unsymmetrical relativistic eikonal approximation for collision energies below 10 GeV/u [ISE93]. It must be noted, however, that the eikonal theory is a high-energy approximation.

Experimentally the energy dependence of capture has been measured in particular for La^{57+} bare nuclei impinging on a target foil of Au, at collision energies of 0.405, 0.96 and 1.3 GeV/u [BGF+97]. It has been found that the capture cross section falls off approximately as γ^{-3}, similarly indicating that the collision energies considered here belong to an intermediate range, between the high-energy regimes of relativistic and nonrelativistic collisions respectively. The quantitative difference of the exponent of decrease is difficult to account for.

6.3 Charge-number dependence of capture

The dependence of the electron-capture cross section on the charge number of the target and projectile nuclei has been investigated here, for the first time, using the coupled channel method. Numerical calculations have been carried out for a collision energy of 0.96 GeV/u and various symmetrical and unsymmetrical collision systems of heavy nuclei, with charge numbers ranging from $Z_\text{A}, Z_\text{B} = 66$ up to $Z_\text{A}, Z_\text{B} = 92$. As in the previous section, a coupled channel basis comprising the ten lowest bound

states of each centre has been used. For the numerical calculations, the rest frame of nucleus A has been chosen such that cross sections for the target and projectile frames have been obtained. Table 6.5 lists the results for the total cross sections for capture from an initial $1s_{1/2}$-configuration to one of the bound states of the projectile nucleus. The data of this table is plotted in figure 6.7. The corresponding weighted impact-parameter-dependent total capture probabilities $P(b)b$ are shown in the figures 6.8, 6.9 and 6.10 for nine different collision systems.

Discussion. In spite of the manifest differences between the cross sections corresponding to different bases and reference frames, figure 6.5 demonstrates a general tendency of the charge-number dependence of electron capture in heavy ion collisions at 0.96 GeV/u collision energy. For the range of charge numbers consider here, it is observed that the electron-capture cross section grows more strongly with the projectile charge-number, compared to the target charge-number. The increase is not even linear for the target charge-number dependence, and it is slightly stronger than linear for the projectile charge-number dependence.

This result should be compared to the Z_T-Z_P-dependence of other relativistic capture theories that are based on perturbation theory. Roughly, most capture theories predict, for large collision energies, a charge-number dependence of nonradiative electron-capture according to, $\sigma_{\text{capture}} \propto Z_T^5 Z_P^5$ [EM95]. For a collision energy of 10 GeV/u this behaviour is confirmed by numerical evaluations of cross sections based on the unsymmetrical eikonal approximation [ISE93]. Clearly the present results show a much weaker increase of the cross section with growing target and projectile charge-numbers. In experiments, however, capture from higher atomic shells, which

TABLE 6.5. Total capture cross sections $\sigma_{\text{capture}}(1s_{1/2})$ as a function of the projectile and target charge numbers, Z_T and Z_P, for a collision energy of 0.96 GeV/u. The cross sections are given in kbarn. The columns are subdivided to distinguish between results obtained in the target (tar.) and projectile (proj.) frames respectively. Similarly the rows are subdivided in order to present the data obtained from calculations with undistorted and phase-distorted basis functions. The cross sections have been obtained from coupled channel calculations with the ten lowest bound states of each nucleus and are plotted in figure 6.7.

	Z_P	92 (U)		86 (Rn)		79 (Au)		66 (Dy)	
Z_T		tar.	proj.	tar.	proj.	tar.	proj.	tar.	proj.
92 (U)	undist.	1.295	1.465	1.115	1.230	0.908	0.961	0.555	0.533
	ph.-dist.	1.355	1.198	1.128	0.995	0.873	0.767	0.475	0.412
86 (Rn)	undist.	1.235	1.402	1.080	1.187	0.890	0.939	0.553	0.535
	ph.-dist.	1.231	1.080	1.035	0.906	0.811	0.708	0.452	0.390
79 (Au)	undist.	1.102	1.266	0.975	1.083	0.812	0.868	0.513	0.507
	ph.-dist.	1.043	0.908	0.885	0.770	0.703	0.610	0.401	0.344
66 (Dy)	undist.	0.792	0.907	0.710	0.788	0.597	0.643	0.387	0.390
	ph.-dist.	0.652	0.563	0.562	0.486	0.455	0.394	0.270	0.232

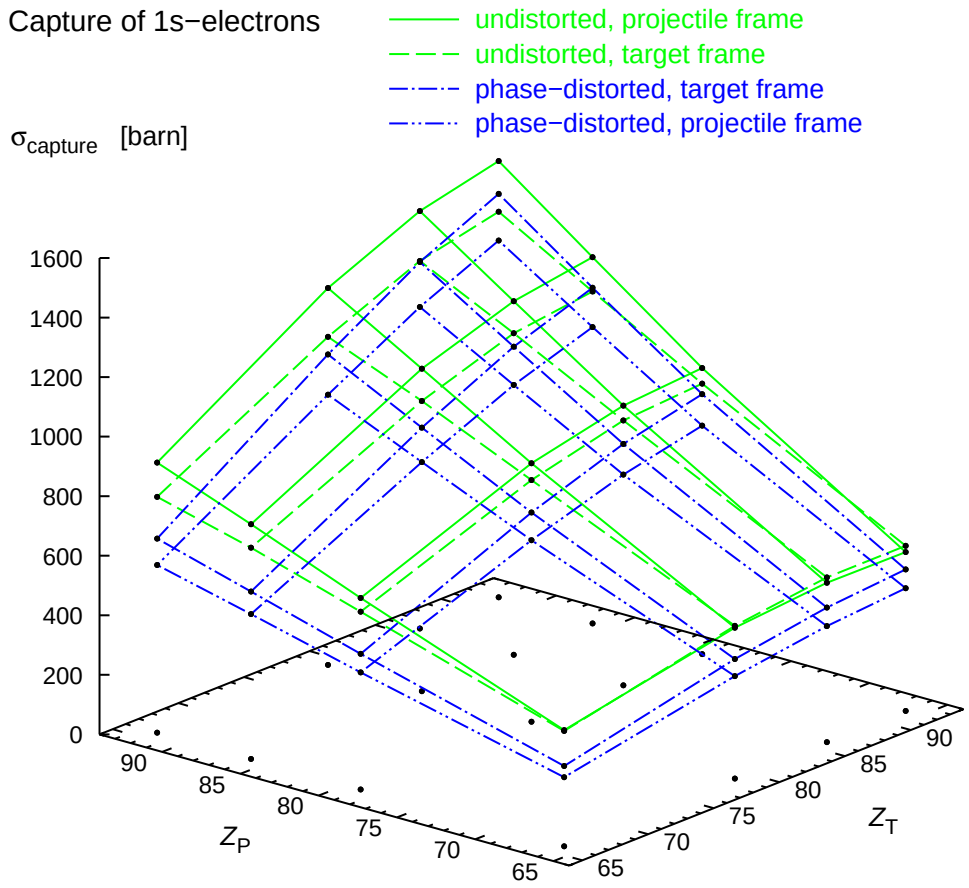

FIGURE 6.7. The dependence of the total cross section of 1s-electron-capture on the charge numbers Z_T and Z_P of the target and projectile nuclei respectively is presented here. The data has been obtained by integrating the interpolating functions of the figures 6.8, 6.9 and 6.10, and additional data for the remaining collision systems involving $Z_T = 86$ or $Z_P = 86$. It is clearly discernible that the capture cross section grows more strongly for growing Z_P compared with the dependence on Z_T.

is not considered here, becomes more important for larger charge numbers. Therefore, the presently found slow increase of the capture cross section, as a function of the charge numbers Z_T and Z_P, presumably underestimates the charge-number dependence of experimentally determined total cross sections of (nonradiative) electron capture slightly.

In [BGF+97] measurements of electron capture by U^{92+}-ions impinging on solid target foils of Cu, Ag and Au have been reported. The collision energy was 0.96 GeV/u and is, therefore, identical to the collision energy of the present numerical calculations. It has been found that the existing perturbation theory of electron capture was able to account for the measured cross sections for the targets Cu and Ag. But for the Au target the total cross section obtained from perturbation theory overestimated the experimental value of 3.4 kbarn by about 20% (see figure 5 in [BGF+97]). The

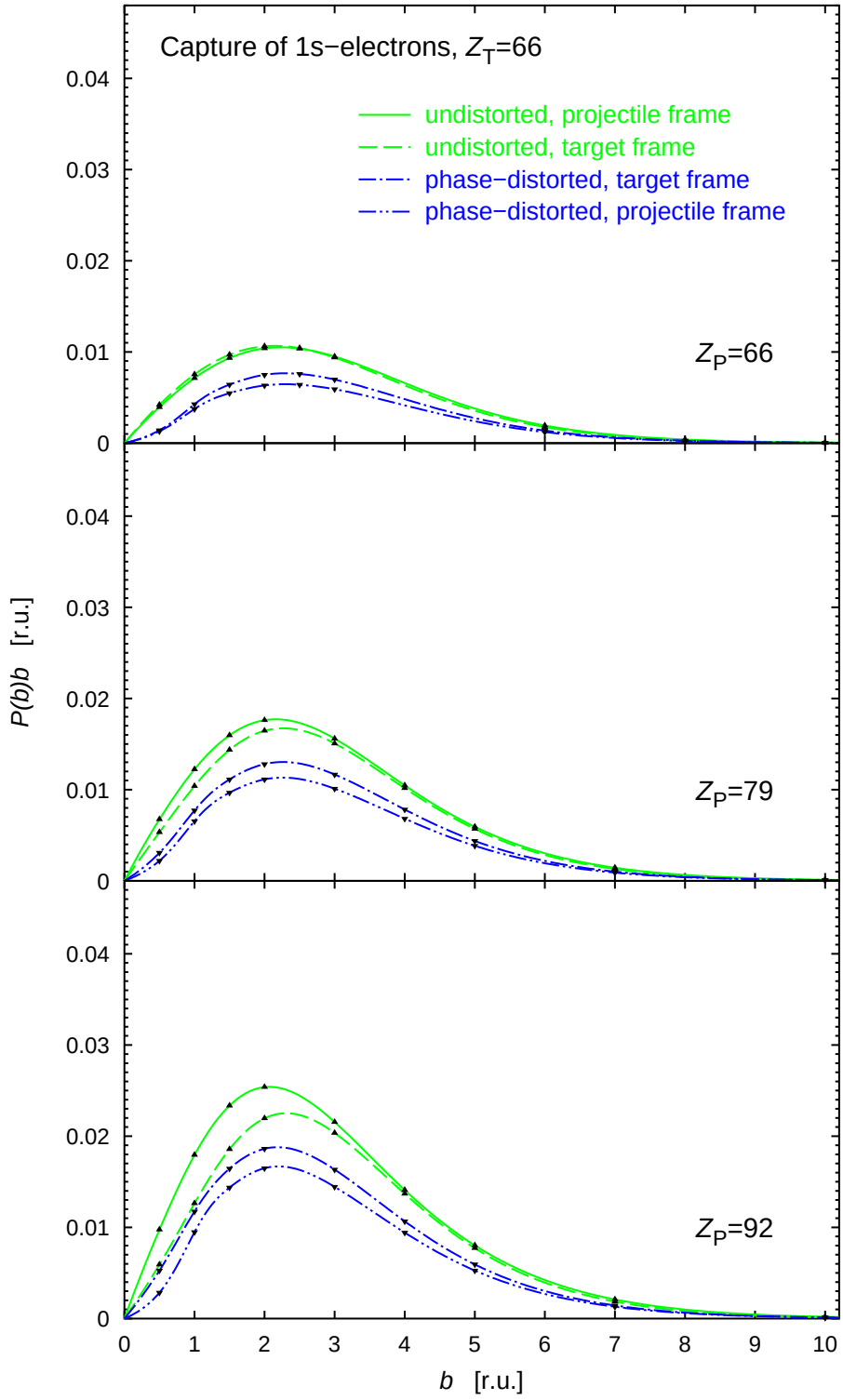

FIGURE 6.8. The impact parameter dependence of electron capture for a collision energy of 0.96 GeV/u is presented here for nine different heavy-ion collision systems. The data has been computed by relativistic coupled channel calculations employing the 10 lowest bound states of each nucleus. The initial configuration is a 1s-state of the target nucleus with charge number Z_T. Four different series' of calculations, performed in the rest frames of the target and the projectile respectively, using either undistorted or phase-distorted asymptotic states, are shown (see the text for explanations).

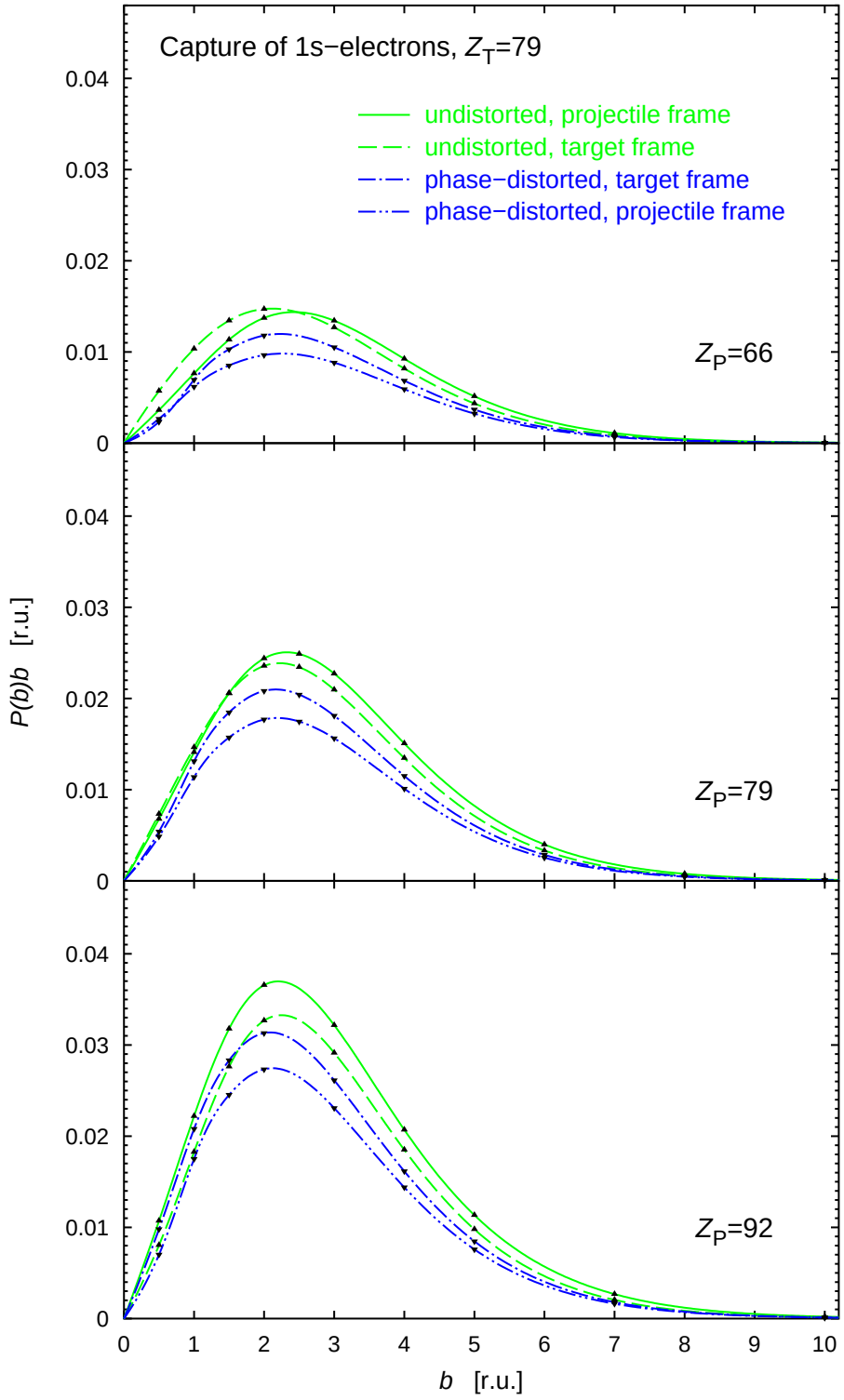

FIGURE 6.9. (See figure 6.8)

present calculations roughly support these experimental findings, namely that the charge-number dependence of the nonradiative capture cross section is overestimated by the perturbative theories, if collisions of *heavy* ions at intermediate relativistic energies are considered.

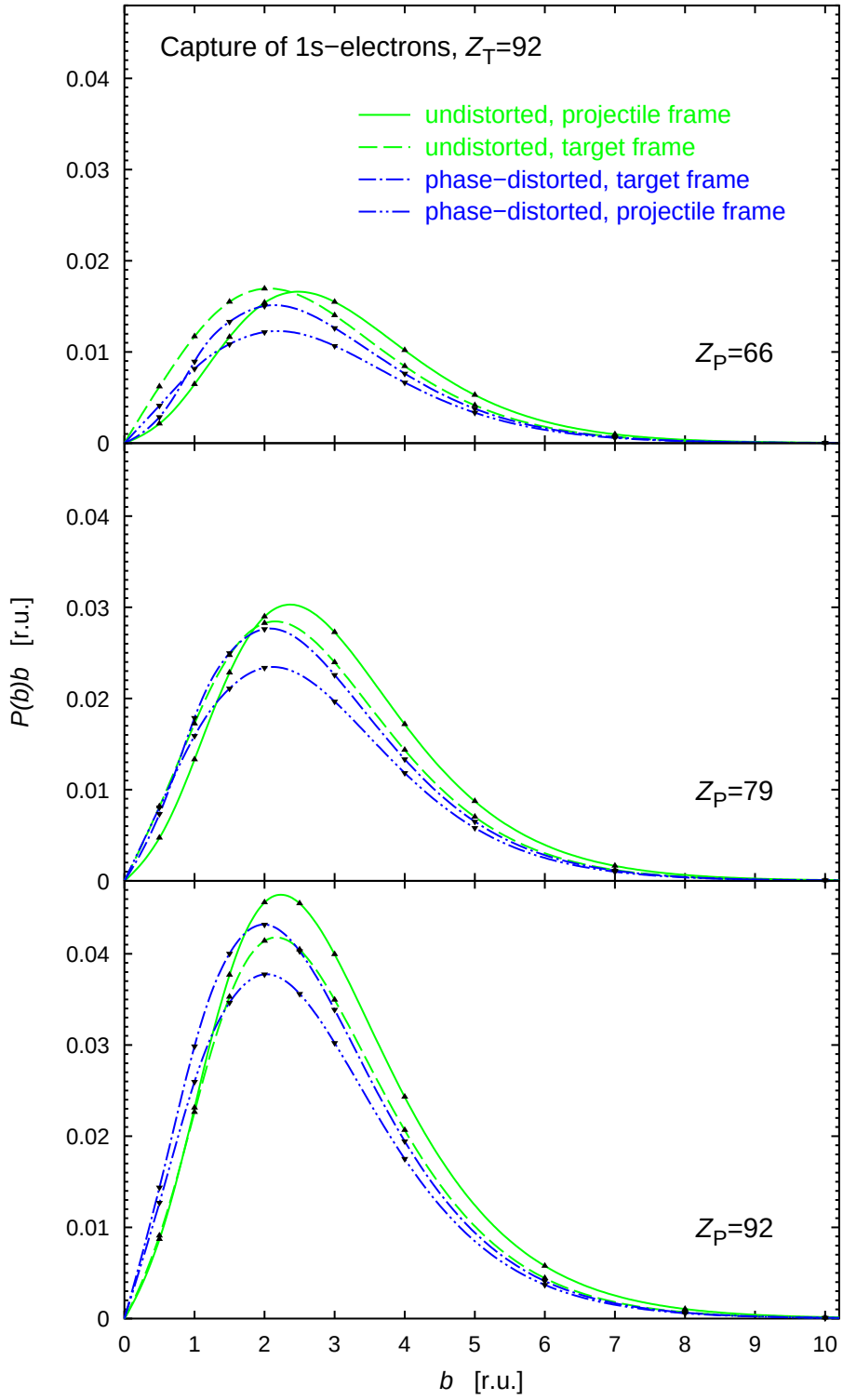

FIGURE 6.10. (See figure 6.8)

A direct comparison of the measured cross section with the present numerical results is not straightforward, since the coupled channel method allows for target excitations, which are not possible in solid targets. Moreover the measured cross section of 3.4 kbarn, for the collision U^{92+} + Au, comprises the process of radiative electron

capture, contributing approximately 1.0 kbarn (according to [BGF+97]). Nevertheless, the presently determined value for electron capture from a filled target-K-shell is roughly 2 kbarn (cf. table 6.5) and the remaining difference to the experimental value may convincingly be ascribed to nonradiative capture from higher target-shells.

Regarding the systematic difference between calculations with an undistorted and with a phase-distorted basis in figures 6.7–6.10, note, however, that cross sections obtained from calculations with undistorted basis functions in the *collider* frame are expected to be smaller than those of the target and projectile frames. This fact has been established in the preceding sections.

6.4 Frame dependence

The aim of this section is to elucidate further the influence of the choice of the reference frame on two-centre coupled channel calculations.

6.4.1 Continuum of reference frames. For a sequence of different reference frames, the total capture probability is shown in figure 6.11, for transitions from initial 1s- or 2s-configurations to an arbitrary bound state of the projectile nucleus. Again, the calculations have been done using a basis comprising the ten lowest bound states of each nucleus. The parameter used to characterise the different reference frames, employed for the coupled channel calculations, is the following fraction of the target and projectile rapidities, χ_{T} and χ_{P}, in $\boldsymbol{e}_3$-direction (cf. section 5.1):

$$\xi = \frac{\chi_{\mathrm{T}} + \chi_{\mathrm{P}}}{\chi_{\mathrm{T}} - \chi_{\mathrm{P}}}. \tag{6.2}$$

Clearly, $\xi = 0$ corresponds to the collider frame, and $\xi = -1$ and $\xi = 1$ to the target and projectile frames respectively. If the modulus of ξ is greater than one, then both centres are moving in the same direction with different absolute velocities. The value for the impact parameter $b = 2$ r.u. chosen for the calculations shown in figure 6.11, approximately coincides with the maximum of the $P(b)b$-plots presented in the previous sections. Note as well that the K-shell radius of uranium is approximately 1.5 r.u., representing a typical length scale of the collision system considered in figure 6.11.

Figure 6.11 exhibits the strong frame dependence of capture probabilities obtained from coupled channel calculations using exclusively undistorted bound-state basis functions. The uncertainty of the results for the initial 1s-configuration is nearly of the same order of magnitude as the probability itself. This has not been noted before in the literature. The solid green line, corresponding to calculations with phase-distorted bound-state basis functions, shows a much weaker dependence on the reference frame of the calculation. This fact, anticipated already in section 6.1, suggests that a coupled channel expansion with phase-distorted basis functions yields a better approximation to the exact solution of the two-centre Dirac equation, than an expansion using the same number of undistorted states.

6.4.2 Time axes in relatively moving frames. For three different frames of reference, the green dashed lines in figure 6.12 show the deviation of the overlap matrix $N(t)$ from the unit matrix, as measured by the Frobenius norm $\|N(t) - 1\|_{\mathrm{F}}$

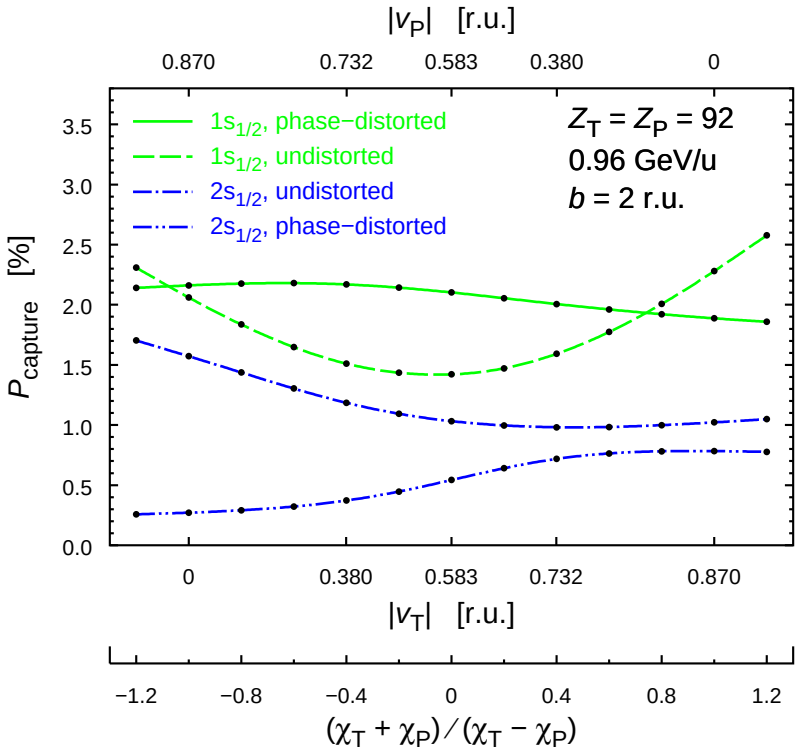

FIGURE 6.11. Total capture probabilities $P(b)$ in thirteen different reference frames and for two different initial configurations are shown. The data was obtained by coupled channel calculations employing the 10 lowest bound states of each centre, either with undistorted or phase-distorted basis functions. The charge numbers are $Z_\mathrm{T} = Z_\mathrm{P} = 92$, the impact parameter is $b = 2\,\mathrm{r.u.}$ and the kinetic energy 0.96 GeV/u in all calculations. Apart from the axis for the ratio of rapidities $(\chi_\mathrm{T}+\chi_\mathrm{P})/(\chi_\mathrm{T}-\chi_\mathrm{P})$, which is used to characterise the various reference frames, two further abscissa axes are provided for the velocities of the centres. The values -1, 0 and 1 of the ratio $(\chi_\mathrm{T}+\chi_\mathrm{P})/(\chi_\mathrm{T}-\chi_\mathrm{P})$ correspond to the target, collider and projectile frames respectively.

(see section 5.4). The time interval of a non-vanishing Frobenius norm represents the time interval during which the basis functions of different centres overlap and, thereby, relates the time axes of different coordinate systems. It is seen that the reference frame with the shortest overlap time (the 'fastest collision') is the collider frame. In other frames the overlap time is longer. A short calculation, taking into account the Lorentz contraction of bound-state basis functions and the relative speed of the centres, yields that the overlap time is 'dilated' with respect to the collider frame approximately by the following factor:

$$\cosh\left(\frac{\chi_\mathrm{A}+\chi_\mathrm{B}}{2}\right). \tag{6.3}$$

This relationship among the time axes of relatively moving frames is qualitatively exhibited by figure 6.12.

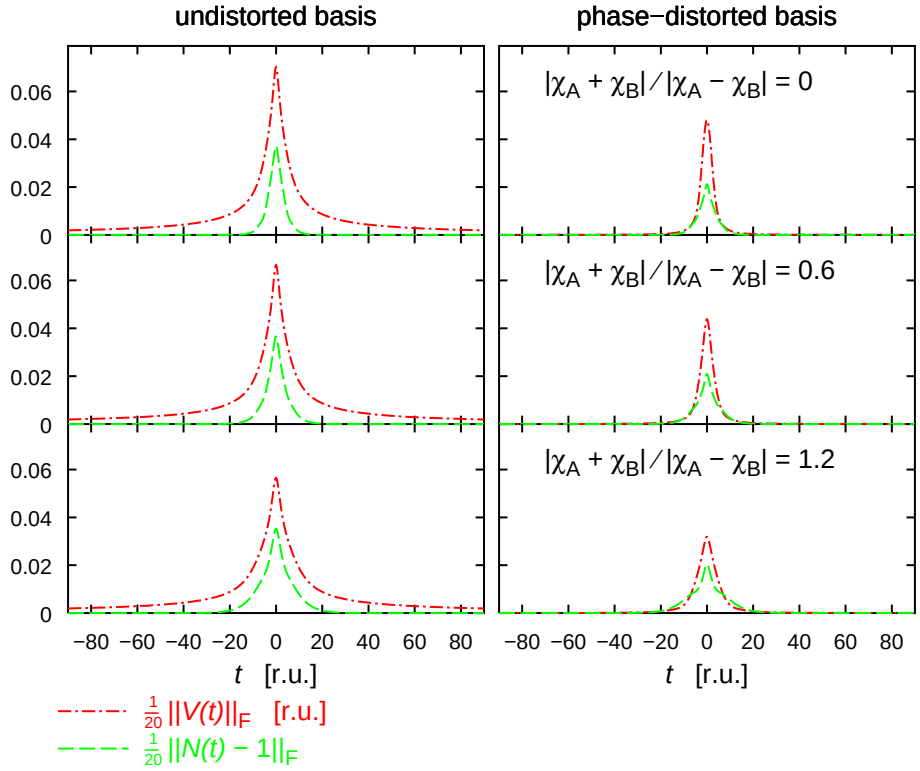

FIGURE 6.12. This figure illustrates the relation of the time axes of different relatively moving reference frames. The parameters for the coupled channel calculations, presented here, are same as in figure 6.11. The width of the green curve, representing the Frobenius norm of the matrix $N(t) - 1$, characterises the time interval in which the basis functions of different centres significantly overlap. It is seen that in calculations with phase-distorted basis functions the interaction matrix $V(t)$ is essentially vanishing outside this time interval. Contrary, the interaction matrix elements with undistorted basis functions are only slowly decreasing as $\pm t$ increases.

6.5 Coulomb boundary conditions

In this section we show that Coulomb boundary conditions take effect in arbitrary reference frames.

From figure 6.12 it is inferred as well that Coulomb boundary conditions, i.e. the use of phase-distorted basis functions, lead to a short-range interaction in any reference frame considered in numerical calculations (cf. section 3.7). More precisely, in calculations with phase-distorted basis functions the matrix elements of the interaction matrix $V(t)$ decrease much faster to zero as time increases (or decreases), compared to calculations using undistorted bases. This verifies the efficacy of the Coulomb boundary conditions in arbitrary reference frames.

Finally, turn to the figures 6.13 and 6.14. The time-evolution of the squared moduli of the coefficients $c_i(t)$ is shown for the target and projectile frames, and two other frames of reference, in which the centres are moving with different velocities and in opposite directions. The initial configuration is a $1s_{1/2}$-state of centre A, the latter taking, therefore, the role of the target. Again, the collision system considered

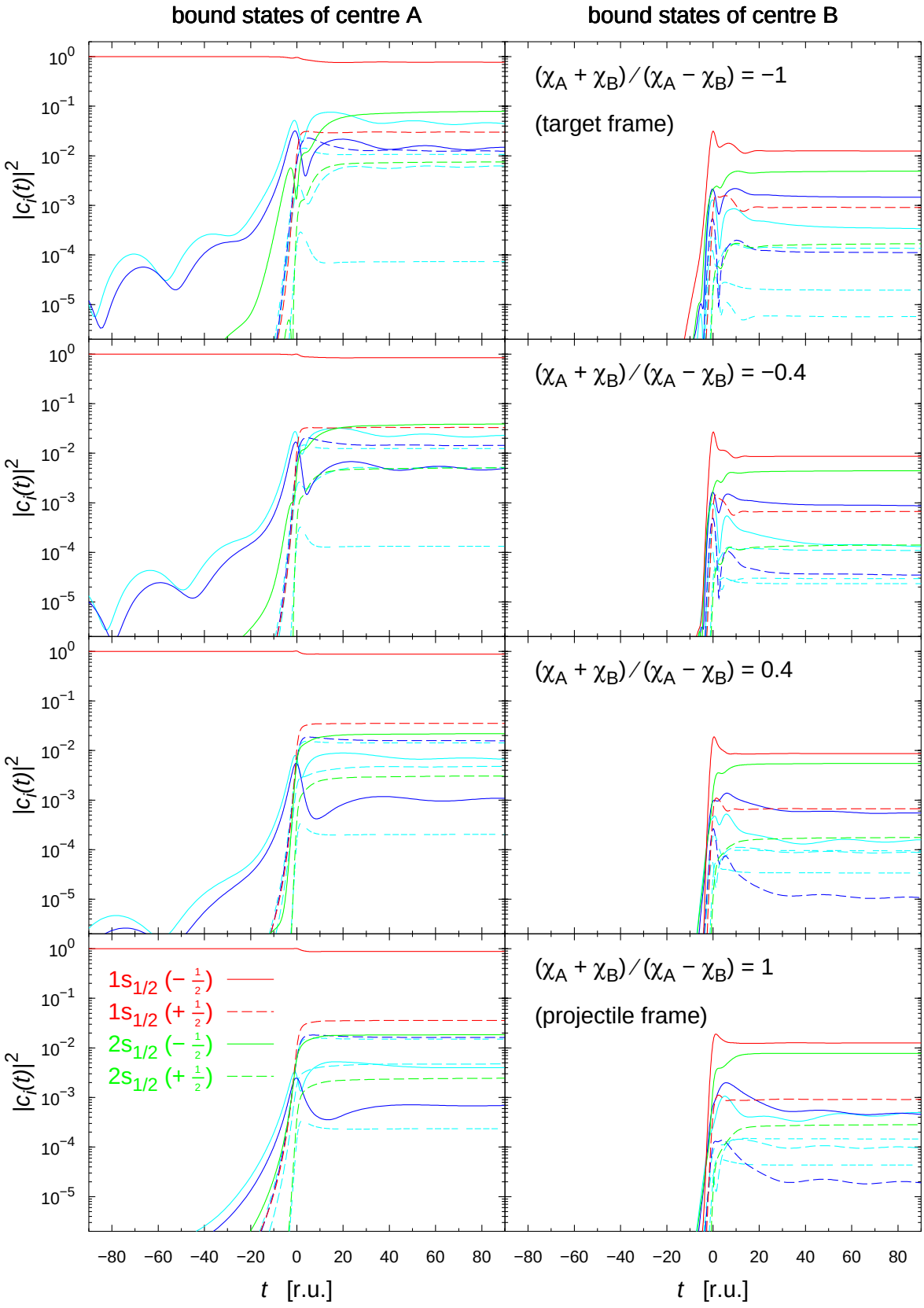

FIGURE 6.13. The time evolution of the squared moduli of the expansion coefficients $c_i(t)$ obtained from coupled channel calculations with *undistorted* basis functions, in four different reference frames. The initial configuration is a $1s_{1/2}$-state of nucleus A. The allocation of line styles to basis functions is the same as in figure 5.1 on page 55. Parameters which are common to all four calculations are: $T = 0.96\,\mathrm{GeV/u}$, $b = 2\,\mathrm{r.u.}$ and $Z_\mathrm{T} = Z_\mathrm{P} = 92$. They are, therefore, identical to those of figure 6.11.

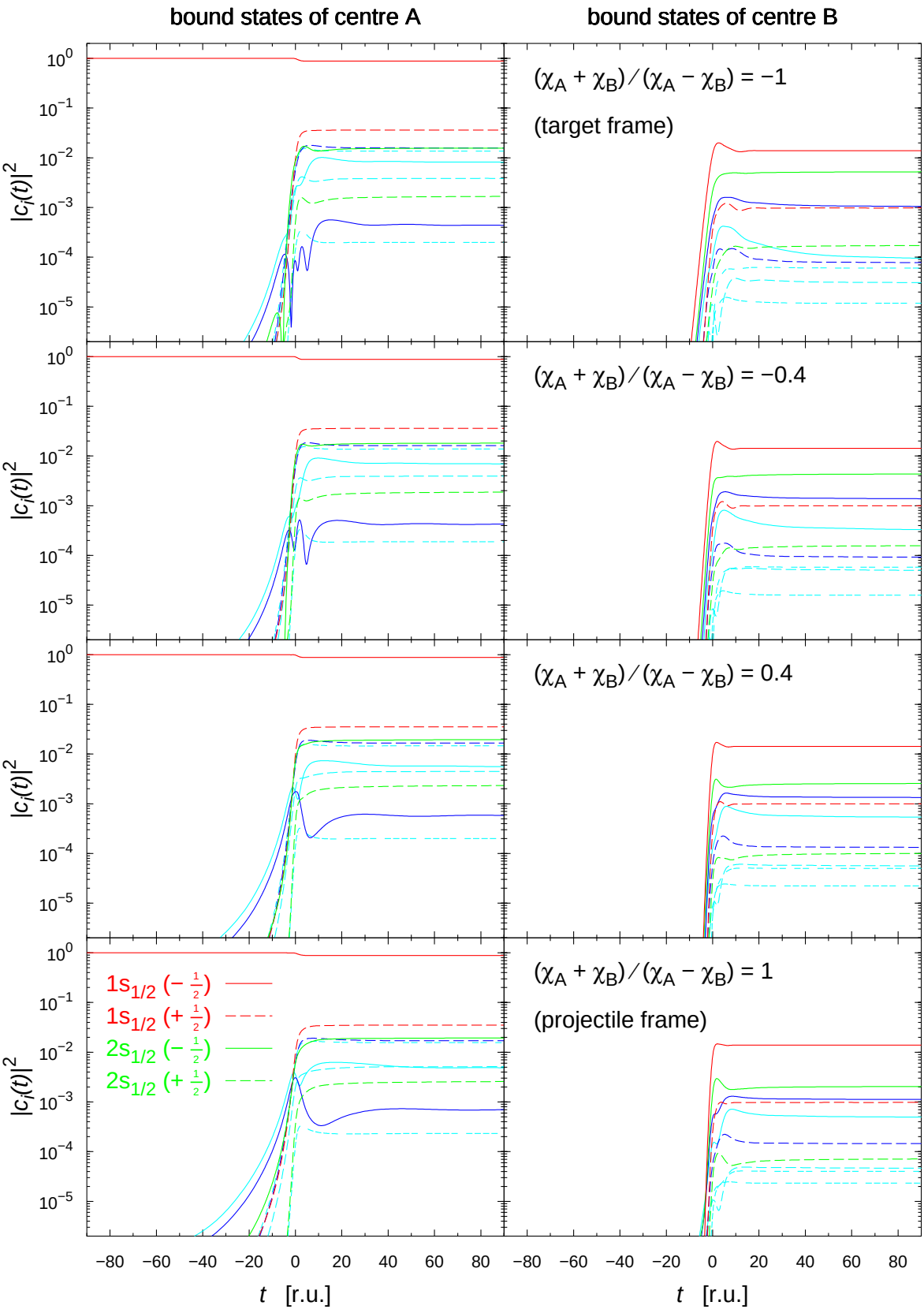

FIGURE 6.14. As figure 6.13, but for calculations with *phase-distorted* basis functions.

is $Z_A, Z_B = 92$ at a collision energy of $T = 0.96\,\mathrm{GeV/u}$, with an impact parameter of $b = 2\,\mathrm{r.u.}$. In fact, the plots take another view on the same calculations, also presented in the figures 6.11 and 6.12.

A distinctive feature of figure 6.13, showing results obtained with an undistorted basis, is the existence of long-range target excitations for the target-frame calculation. Gradually passing over to the projectile frame, the extent of the target excitations decreases. Correspondingly, oscillations between the projectile states, after the collision, become increasingly visible, and they are greatest in the projectile frame. Qualitatively this can be understood as follows: since the excitation of target states is mainly caused by the magnetic field of the projectile [TE90, EM95], these excitations are, hence, vanishing in the projectile frame. Similarly, in the projectile frame, the target nucleus causes long-range interactions between projectile bound-states.

A detailed analysis of state-differential cross sections of electron excitation and transfer is not presented in this thesis. The reason is the extraordinary frame dependence of the transition probabilities, clearly exhibited in figure 6.13. For this series of calculations, using undistorted basis functions in various reference frames, some transition probabilities vary over more than one order of magnitude. It has been checked that this is not a spurious effect, due to the finite time interval $[t_i, t_f]$ of numerical calculations, but is a clear signature of the violation of the Lorentz invariance as a consequence of the coupled channel ansatz. In particular, it was found that the initial and final times t_i and t_f of a numerical calculation may be chosen shorter than reported in [TE88A], thereby reducing computational effort without loss of accuracy.

This frame dependence of single transition-amplitudes is less vigorous for the calculations with phase-distorted basis functions, reflecting the similar behaviour of the total capture probabilities, which was discussed already. At first glance, it might seem surprising that the excitation of target bound-states, in calculations performed with undistorted and phase-distorted bases in the *projectile* frame, is nearly identical. This fact is observed by comparison of the bottom plots of the figures 6.13 and 6.14. But, as stated above, the use of Coulomb boundary conditions mainly removes the long-range part of the projectile magnetic-field, the bound states of the target nucleus are exposed to. Clearly, the latter does not exist in the projectile frame.

6.6 Bound-free pair creation

In this section, results from coupled channel calculations with free-particle basis functions are presented. These calculations required much computing time and have been feasible only as distributed multiple-processor computations.

The main motivation for the present choice of free-particle basis functions has been explained in section 5.5. In the literature relativistic coupled channel calculations of bound-free pair creation have been reported by several authors [RMS$^+$91, MGS91, RSG93, BRBW93, BRBW94]. All of these use a *single*-centre basis of bound states and wave packets. Therefore, these calculations can only describe excitation-like processes (cf. figure 5.6). In the present approach we make an attempt to allow for the description of excitation- and transfer-like processes at the same time by using a two-centre basis (cf. figure 5.7).

Bound-free pair production has been observed first in heavy-ion collisions with collision energies in the 1 GeV/u energy range [BGF+93, BGF+94]. The experimentally found cross sections for this process could not be explained reliably by existing theoretical descriptions [BGF+97], namely perturbation theories, single-centre coupled channel calculations or nonperturbative numerical solutions of the two-centre Dirac equation in momentum space [MBS95, MBS96]. Discrepancies have been reported for the absolute value of the total cross section and its dependencies on nuclear charge numbers and the collision energy. The agreement between observation and perturbative calculations is more satisfactory at higher collision energies of about 10 GeV/u [BCD+98]. It has been proposed that the discrepancy at intermediate energies is due to two-centre effects, not accounted for in usual perturbative calculations or single-centre coupled channel approaches.

The aim of the present calculations is not to determine cross sections, in better agreement with experiment than cross sections obtained by the previous theoretical approaches. This cannot be expected because of our very limited basis size due to numerical constraints. Instead, we attempt to assess the relative importance of the transfer-like pair creation process, neglected in single-centre approaches, compared to the excitation-like mechanism. In other words, the aim is to get a qualitative insight into two-centre effects in bound-electron free-positron pair creation at intermediate relativistic collision energies.

It has been proposed in [Eic95, ED96, IE96] that apart from familiar excitation-like processes also transfer-like processes contribute to the cross section of bound-free pair creation. In these articles, perturbative calculations are reported treating bound-free pair creation as a charge-transfer process. Note that perturbative treatments must take either point of view and cannot combine both mechanism. In the calculations a different asymptotic energy dependence of the total cross section, compared to the usual perturbative treatment of bound-free pair production as an excitation-like process, was obtained. However, a unified treatment of excitation- and transfer-like pair creation processes, as depicted in figure 5.7, is not feasible in the framework of perturbation theory. It has been attempted in the present work by means of a coupled channel approach.

In the following, results from coupled channel calculations for the collision system $Z_A, Z_B = 92$ at a collision energy of 0.96 GeV/u and 1 GeV/u respectively are presented. Most coupled channel bases comprise the ten lowest bound states of each nucleus. Furthermore, Lorentz-transformed stationary wave-packets of the form (5.19) are included, either for one centre or for both centres. For the reason of computational feasibility the parameters, defining the free-particle basis functions (5.19), have been chosen according to:

$$\begin{aligned} \kappa &= \pm 1, \\ \Delta_\epsilon &= 0.3\,\text{r.u.}, \\ \bar{\epsilon} &= \pm 1.15, \pm 1.45, \pm 1.75\,\text{r.u.}. \end{aligned}$$

For each centre, these parameters yield 24 free-particle basis functions, half of them with positive energy and the other half with negative energy. The radial wave functions of these wave packets are approximately localised within a sphere of 200 r.u.

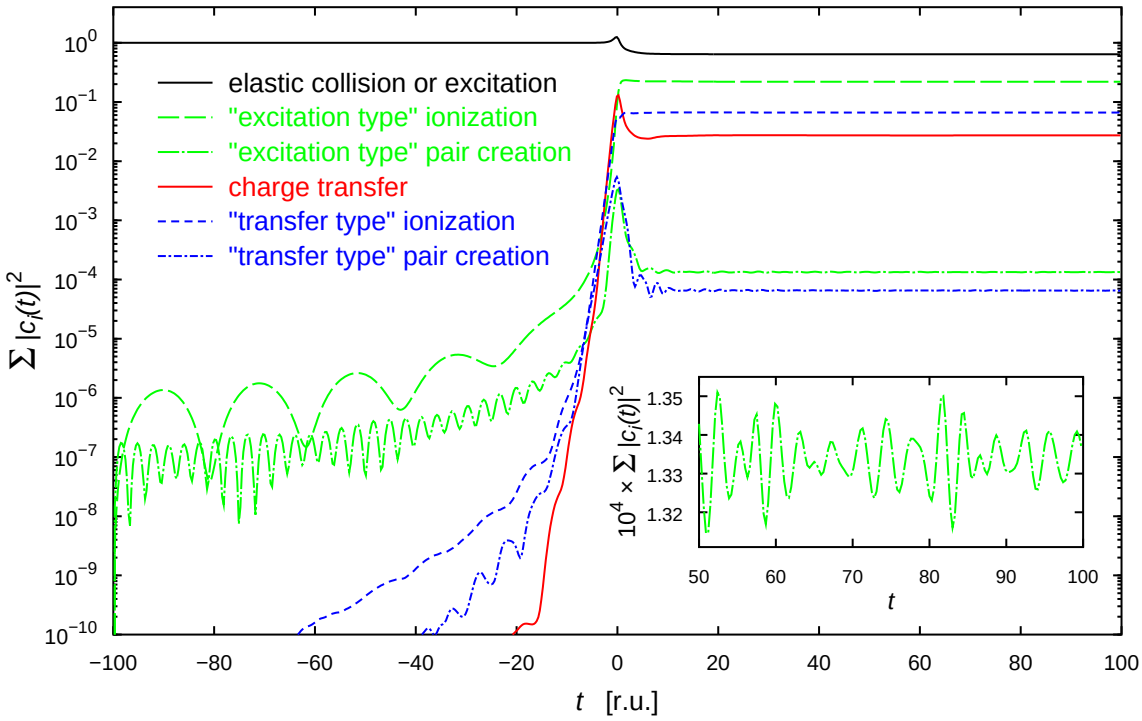

FIGURE 6.15. Time evolution of the sums over squared moduli of the expansion coefficients $c_i(t)$. The sums are taken over those coefficients which correspond to the same atomic process. For large times t these sums yield the probabilities of the respective processes, as indicated in the legend (see figure 5.7 as well). The charge numbers are $Z_A, Z_B = 92$ and the collision is taking place at a collision energy of $T = 1\,\mathrm{GeV/u}$ with an impact parameter of $b = 0.5\,\mathrm{r.u.}$. The data shown here has been computed by a coupled channel calculation in the collider frame using 68 basis functions. The initial configuration is a $1s_{1/2}$ bound state. Due to the long-range character of the Coulomb interaction, oscillations of the coefficients are present, for large negative as well as positive times. The inset shows these oscillations for the probability of the excitation-like bound-free pair creation process.

(with respect to their respective rest frames) and have been cut off outside this volume. They are oscillating functions and, therefore, the numerical evaluation of matrix elements, in particular of the two-centre interaction and overlap matrix elements, becomes computationally more demanding in comparison with matrix elements involving only bound-state basis functions.

It should be noted that the mean energies $\bar{\epsilon}$ of these wave packets are too small to account for the experimentally observed electron and positron energy spectra [BGF+97]. Therefore, results of the present coupled channel calculations are generally not expected to yield cross sections of bound-free pair creation in quantitative agreement with experiment. The present emphasis is on a qualitative understanding of two-centre effects in pair creation. In addition, the frame dependence of the coupled channel calculations is studied.

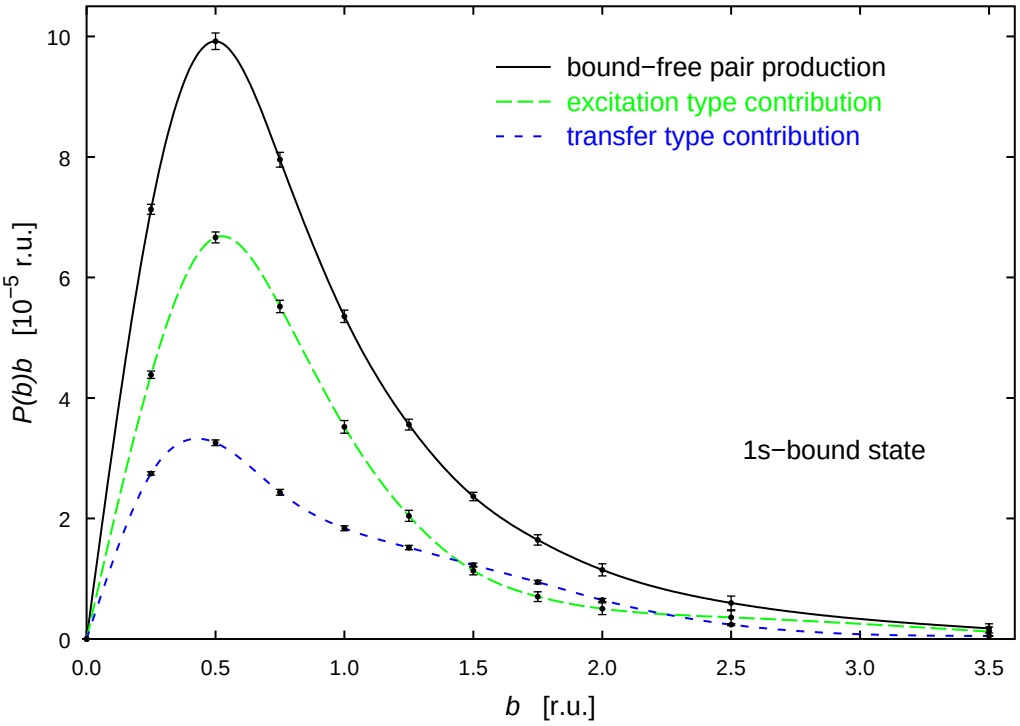

FIGURE 6.16. Weighted probabilities for bound-electron free-positron pair creation as a function of the impact parameter, obtained from coupled channel calculations in the collider frame using a two-centre basis of 68 basis functions. The collision energy is 1 GeV/u and the results shown refer to a collision of two bare uranium nuclei. The electron is created in a $1s_{1/2}$ state of one of the nuclei.

6.6.1 Collider frame calculation. Coupled channel calculations with a symmetrical basis, comprising the ten lowest bound states and 24 wave packets at each centre, have been performed for a series of impact parameters in the collider frame. A collision energy of 1 GeV/u was chosen and the calculations have been done using an undistorted basis. Figure 6.15 shows the time evolution of the sum of the squared moduli of expansion coefficients $c_i(t)$, which belong to the same scattering channel. It is distinguished between excitation-like and transfer-like processes for the free-particle scattering channels, in accordance with figure 5.7. The initial configuration is a $1s_{1/2}$ bound state of centre A. Transition amplitudes to bound states of centre B are interpreted as charge-transfer amplitudes (red line). Transitions to wave packets of positive energy are attributed to either excitation-like or transfer-like ionisation (green and blue dashed lines). Finally, transition amplitudes to wave packets of negative energy are interpreted as bound-free pair creation amplitudes (green and blue dashed-dotted lines) (cf. section 3.6).

Figure 6.15 clearly exhibits the long-range character of the Coulomb potential leading to a coupling of the initial state to wave packets of negative and positive energy of centre A, much before the closest approach of the centres at time $t = 0$. These couplings are present also for the outgoing channels, leading to oscillations of the probabilities at large times t. These oscillations are shown, as an example, for the excitation-like pair creation probability and the time interval $t = 50 \ldots 100$ r.u.

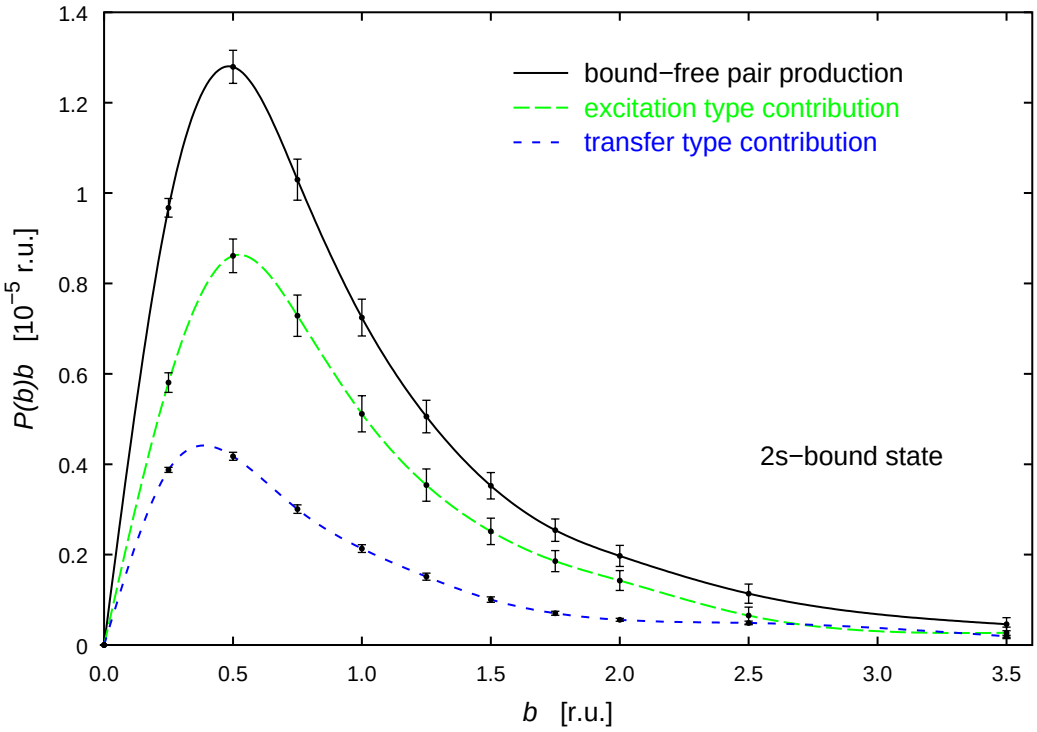

FIGURE 6.17. As figure 6.16, but the electron is created in a $2s_{1/2}$ bound state of one of the colliding nuclei.

by the inset of figure 6.15. It is seen that the amplitude of these oscillations is small and that there is no shift of the mean value as time increases.

The presence of these oscillations demonstrates another numerical complexity: The time steps for the numerical integration of the coupled channel equations (4.8) have to be chosen much smaller, compared to the computationally less demanding pure capture calculations, discussed in the previous sections. If wave packets of higher energy $\bar{\epsilon}$, than considered here, were used, not only the evaluation of matrix elements becomes more involved, but also the time-integration of the coupled equations becomes even more demanding.

Figure 6.16 shows the weighted probabilities for bound-free pair creation, in which the electron is created in a $1s_{1/2}$ bound state. The different contributions from excitation- and transfer-like pair creation probabilities are given, the total probability of bound-free pair creation just being the sum of these two contributions. It is discernible that excitation- and transfer-like processes are of similar relative importance, the excitation-type process being favoured. Note that the maximum of the weighted pair creation probability $P(b)b$ is at an impact parameter $b = 0.5\,\text{r.u.}$. Compared to the charge transfer process, the the main contribution to the pair-creation cross section comes from smaller impact parameters, due to the great field strength necessary for pair production.

Figure 6.17 shows the analogous plot for bound-free pair production, in which the electron is created in a $2s_{1/2}$ bound state. The corresponding weighted probabilities are approximately one order of magnitude smaller than in figure 6.16. Again it is observed that excitation- and transfer-like processes are of equal importance. The

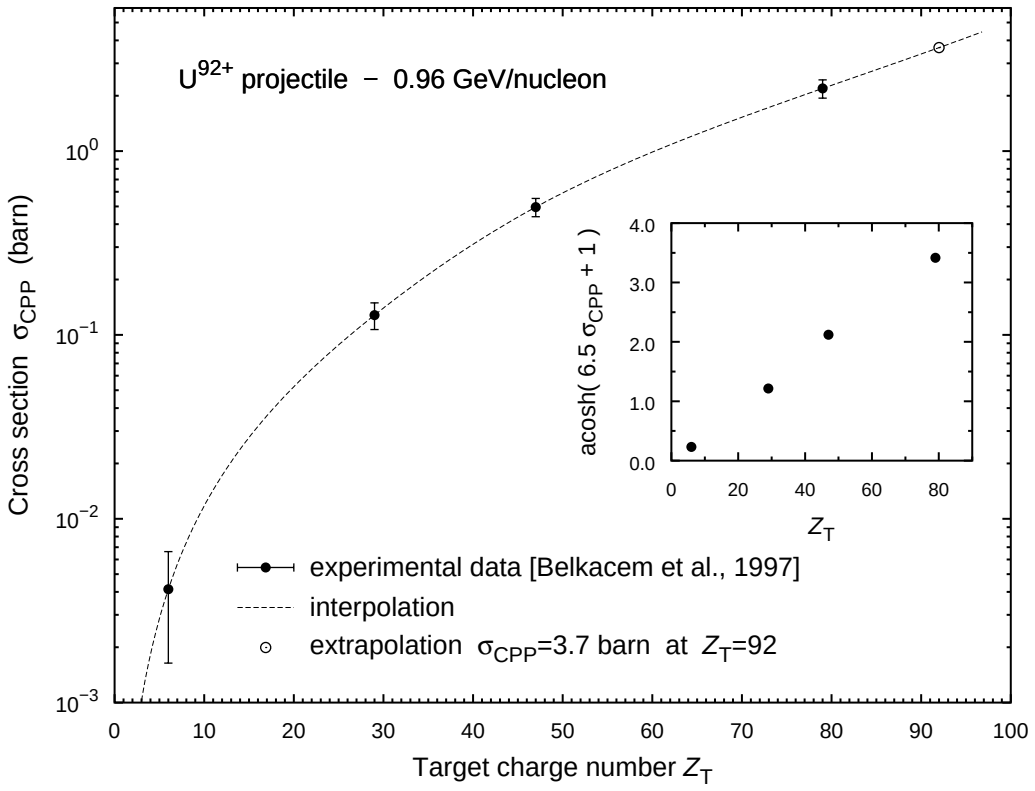

FIGURE 6.18. Linearisation and interpolation of experimental data for bound-free pair creation, as reported in [BGF+97, figure 16]. In the experiment a bare U^{92+} projectile impinged with a kinetic energy of 0.96 GeV/u on solid targets of mylar, Cu, Ag and Au ($Z_T = 6, 29, 47$ and 79). The cross sections are extrapolated to obtain an estimate for a hypothetical solid uranium target.

error bars in both figures, 6.16 and 6.17, represent the amplitude of the oscillations of the final probabilities in the time interval $t = 50 \ldots 100$ r.u. due to the long-range Coulomb interaction, as discussed above.

By integrating the weighted total probabilities of bound-free pair production, shown in the figures 6.16 and 6.17, estimates for the total cross sections of this process are obtained. According to the present rough calculations, for the creation of a $1s_{1/2}$-electron the cross section is 0.95 barn. The corresponding cross section for the creation of a $2s_{1/2}$-electron is 0.13 barn. In fixed target experiments bound electrons can be created only as bound states of the projectile, i.e. of a nucleus of the particle beam in the experiment. Experiments that distinguish specific final states of the created electron are not available yet. The experimentally measured total cross section, therefore, always comprise contributions from all bound states of the projectile. According to the present calculations the contribution of $1s_{1/2}$ states amounts to 2 barn, whereas $2s_{1/2}$ states only contribute 0.2 barn. This reflects a major fraction of the total cross section is due to the creation of $1s_{1/2}$-bound electrons.

6.6.2 Experimental cross section. At this point, we shall compare these calculations briefly with experimental results. In [BGF+97] total bound-free pair creation cross sections for U^{92+} impinging on target foils of mylar, Cu, Ag and Au, at a

collision energy of 0.96 GeV/u, have been reported. These experimental results are plotted in figure 6.18, which partially reproduces [BGF+97, figure 16]. The inset of figure 6.18 shows a linearisation of the experimental data, not noted before. This corresponds to a Z_T^2-dependence of the pair creation cross section for small target charge numbers Z_T, as expected by perturbation theory [EM95, BGF+97].[1] According to this linearisation, the cross section grows exponentially as a function of Z_T for large target charge-numbers Z_T, where perturbation theory is expected to fail. It has been noted already in [BGF+97] that the experimental data is not in agreement with the Z_T^2-dependence predicted by perturbation theory.

This linearisation is presented here, mainly because it is used to extrapolate the experimental data to the collision system $U^{92+} + U$. The interpolation function shown in the main plot of figure 6.18 represents a cubic spline interpolation of the linearised data. The extrapolation of this interpolation function to $Z_T = 92$ yields a cross section of 3.7 barn. Other extrapolation methods give similar values, ranging between 3.5 and 4 barn. It is surprising how close experimental data and the calculation presented in the previous subsection are, taking into account the rather insufficient coupled channel basis. However, a critical judgement might as well regard this coincidence as accidental.

6.6.3 Frame dependence. The calculations in the collider frame using 68 basis functions, presented in subsection 6.6.1, clearly demonstrate that the transfer-like process contributes significantly to the total cross section of bound-free pair creation.

In view of the Lorentz-frame dependence of coupled channel calculations, observed in the capture calculations, it is natural to study the relation between excitation- and transfer-like pair creation also in other computational frames of reference. Coupled channel calculations using the same 68 undistorted basis functions as in subsection 6.6.1 have been carried out in a rest frame of centre A. In this Lorentz frame it must be distinguished, whether the electron is created in a bound state of centre A or centre B. This distinction is not necessary for the collider frame calculation in which the probabilities are the same due to parity conservation.

In this subsection we discuss the plots (1), (2), (6) and (7) of figure 6.19.

In figure 6.19 the plots (1) and (2) show weighted bound-electron free-positron pair creation probabilities, similar to figure 6.16. In plot (1) the electron is created in a $1s_{1/2}$-state of nucleus A, whereas in plot (2) it is created in a $1s_{1/2}$-state of nucleus B. The difference of the results by more than one order of magnitude is striking. The excitation-like pair creation is dominant for the creation of a bound-electron at centre A and the transfer-like process is nearly negligible. By contrast, the transfer-like pair creation mechanism is relatively more important if the electron is created in a bound state of centre B.[2] While passing over from plot (1) of figure 6.19, to figure 6.16, and then to plot (2) of figure 6.19 the excitation-like contribution is

[1] Here Z_T is the charge number of the *experimental target*. In the experiments measuring bound-free pair creation the electron is created in a bound state of the *experimental projectile*.

[2] Remember the following. If the electron is created in a bound state of nucleus B, then the laboratory frame in a fixed-target experiment is identical to the presently considered rest frame of A.

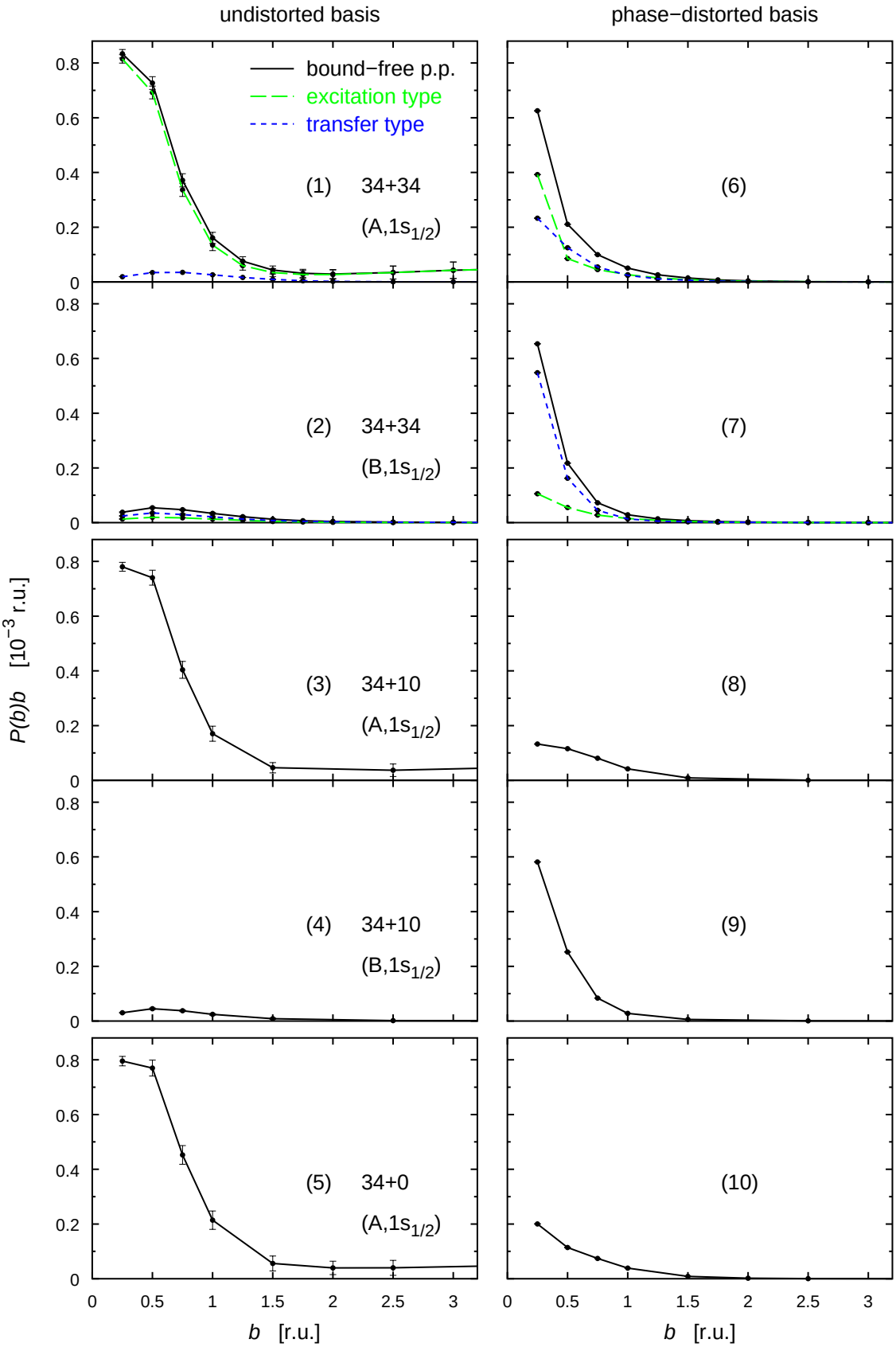

FIGURE 6.19. Weighted probabilities $P(b)b$ for bound-free pair creation, obtained from calculations with free-particle basis functions in the rest frame of centre A, using three different basis sets. All bases comprise the ten lowest bound states and 24 free-particle states of of centre A. The number of basis functions at centre B is varying. The electron is created in a $1s_{1/2}$ bound state of either centre A or centre B, as indicated.

dramatically reducing, showing a similar reduction of excitations as exhibited already by figure 6.13.[3]

The difference of the pair creation probabilities is a numerical artifact, because in a symmetrical collision system the exact probabilities for the creation of a 1s-electron at nucleus A and nucleus B are the same. The reason for this artifact is the very small basis size, which had to be used for numerical reasons. Larger bases might not show such a big frame dependence.

The symmetry mentioned is preserved only by coupled channel calculations in the collider frame, which has been verified. This might suggest that coupled channel calculations performed in the collider frame yield the best results for symmetrical collision systems. Also, experimental data is matched best, by numerical results obtained in the collider frame. On the other hand it is not a priori clear, whether the exact solution of the two-centre Dirac equation is approximated best by a coupled channel ansatz in the collider frame.[4]

The plots (6) and (7) show weighted probabilities obtained from calculations with the corresponding 68 phase-distorted basis functions. The frame dependence of the total pair creation probabilities is much reduced by phase-distorting the basis functions. This resembles the behaviour of the capture calculations. On the other hand the excitation-like process is dominating for the creation of a bound electron at centre A, whereas the transfer-like process is clearly dominating for the creation of a bound electron at centre B. Calculations with phase-distorted basis functions do not exhibit oscillations of the final pair creation probabilities, which are shown in figure 6.15, and which have been observed for the calculations in rest frame of centre A as well, when using an undistorted basis. Note that results obtained with the present, small phase-distorted basis significantly overestimate the experimental cross section of bound-free pair creation.

6.6.4 Two-centre effects. In this subsection, we discuss all plots shown in figure 6.19 and their mutual relation, with an emphasis on two-centre effects.

Single-centre coupled channel calculations and 'semi-two-centre' calculations have been carried out, in order to compare directly the previously discussed results with unsymmetrical representations of the free-particle scattering channel, also reported in the literature [RMS$^+$91, MGS91, RSG93, BRBW93, BRBW94]. Accordingly, these calculations have been performed also in the rest frame of centre A. For the single-centre calculations a basis comprised of the ten lowest bound states and 24 wave packets of centre A has been employed. Semi-two-centre calculations refer to a basis which includes, in addition, the ten lowest bound states of centre B. Clearly, in both cases the free-particle states are always localised at centre A. But as opposed to single-centre calculations, the semi-two-centre calculations allow for the creation of a bound electron at both centre A and centre B. These bases are schematically depicted by figures 5.5 and 5.6.

[3]Note the different scale of the ordinate axes in the figures 6.16 and 6.19.

[4]This reasoning is applicable to the capture calculations of the preceding sections in an analogous way.

It should be mentioned that the single-centre and semi-two-centre bases, used here, only include wave packets, which are at rest in the reference frame of the calculation. Therefore, interpretive difficulties, arising from the slight non-orthogonality of Lorentz-boosted stationary wave packets attributed to the same centre, do not occur (see section 5.5).

First the plots (1), (3) and (5) of figure 6.19 may be compared. It is seen that bound-free pair production, with the creation of an electron in a bound state of centre A, is neither influenced significantly by the presence of the bound states of centre B, nor by the presence the wave packets attributed to centre B. Hence, the effect of the extension of an undistorted single-centre basis by bound states and scattering states of the second centre is not important, in coupled channel calculations in which the created electron is at rest.

By contrast, regarding the fully symmetrical *phase-distorted* basis, the transfer-like pair creation process is relatively more important, as exhibited by plot (6) of figure 6.19. It may be conjectured that this fact is due to a reduced frame dependence of such calculations, as observed already for the pure capture calculations. Omitting the free-particle basis functions of centre B in plot (8) not only removes the possibility for this contribution, but also reduces the magnitude of excitation-like pair creation probability. This is observed also, but less significantly, in plot (10) of figure 6.19, for which the bound states of centre B have been excluded from the basis, too. Hence, the the extension of a *phase-distorted* single-centre basis clearly affects the pair creation probabilities.

The plots (2) and (4), both represent the creation of an electron in a $1s_{1/2}$ bound state of centre B. Their comparison shows that the transfer-like pair creation, already dominant for the fully symmetric calculation with 68 basis functions (cf. plot (2)), is enhanced slightly by the omission of the wave packets of centre B (cf. plot (4)). The qualitatively similar behaviour is observed for the calculations with phase-distorted bases (cf. plots (7) and (9)), which unfortunately yield very different probabilities of bound-free pair creation.

6.6.5 Conclusion. The various calculations do not provide a coherent picture of the importance of two-centre effects in the process of bound-electron free-positron pair creation. The probabilities obtained from calculations in the collider frame are most convincing, because they do not suffer from obvious numerical artifacts, as the violation of the symmetry of electron creation at centre A or B. The collider frame calculations demonstrate the importance of a symmetrical description of the free-particle scattering channel for collisions in the 1 GeV/u collision-energy range. Due to the computational difficulty of the calculations presented, larger coupled channel bases have not been feasible, but they are necessary to avoid the numerical artifacts, like the strong frame-dependence exhibited by figure 6.19.

6.7 Free-particle channels and charge transfer

The coupled channel calculations including free-particle basis functions, as presented in the previous section, also provide probabilities for electron capture. Since this atomic process has been studied extensively in sections 6.1 to 6.4 of this chapter,

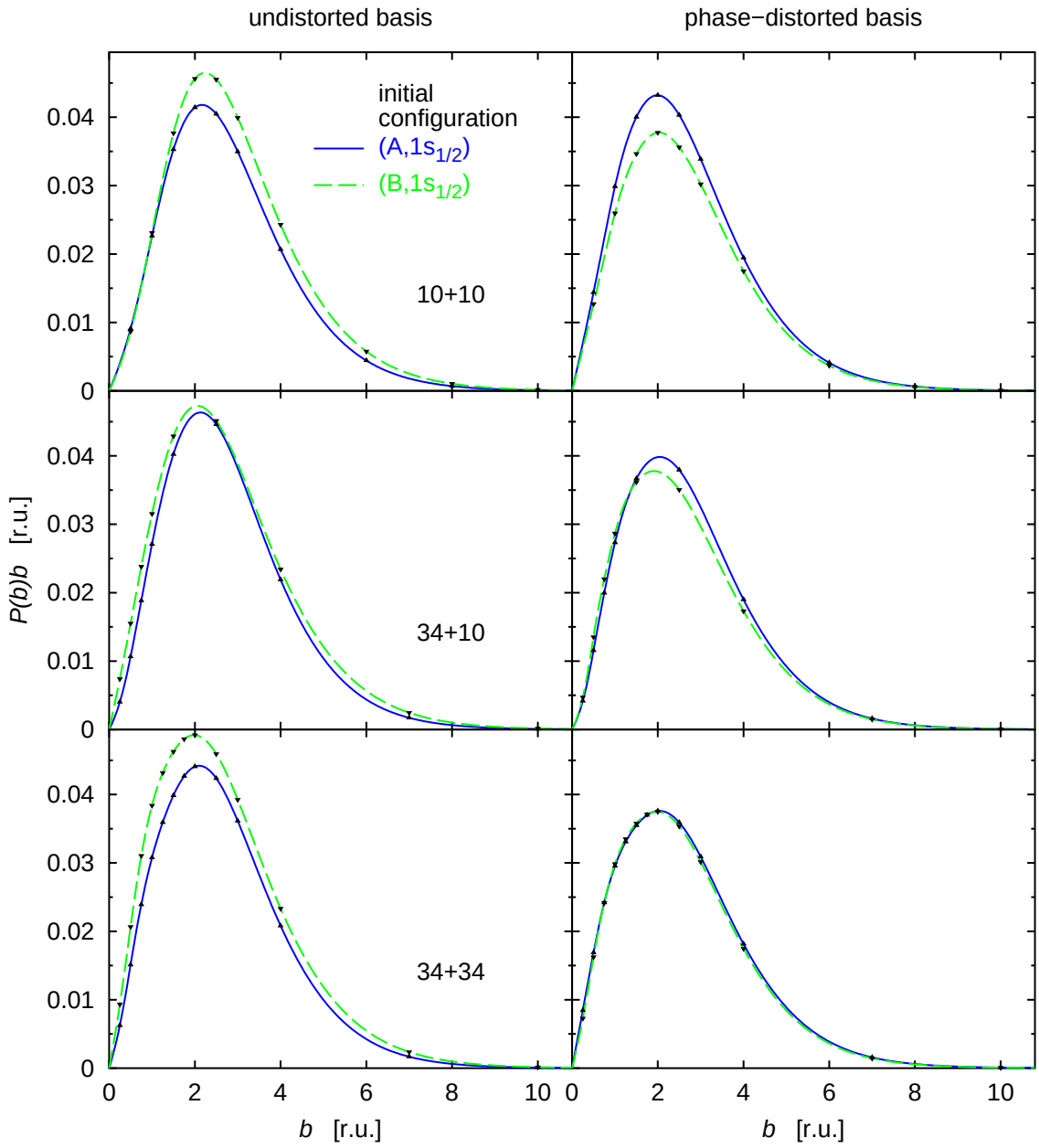

FIGURE 6.20. Weighted total probabilities $P(b)b$ of electron capture for the collision $U^{91+}(1s_{1/2}) + U^{92+}$ as a function of the impact parameter b. The collision energy is 0.96 GeV/u. Results obtained from coupled channel calculations, performed in the rest frame of centre A with six different sets of basis functions, are shown. All bases contain the ten lowest bound states of each centre. The calculations with 68 basis functions, denoted by the label '34+34', comprise stationary wave packets at both centres, as described in section 6.6. The label '34+10' denotes semi-two-centre calculations, in which only stationary wave packets of centre A are included into the coupled channel basis. The addition of free-particle basis functions to the coupled channel basis only comprising bound states (upper two plots) does not have a significant effect on the charge transfer cross section. In calculations with phase-distorted basis functions the inclusion of wave packets clearly reduces the frame dependence.

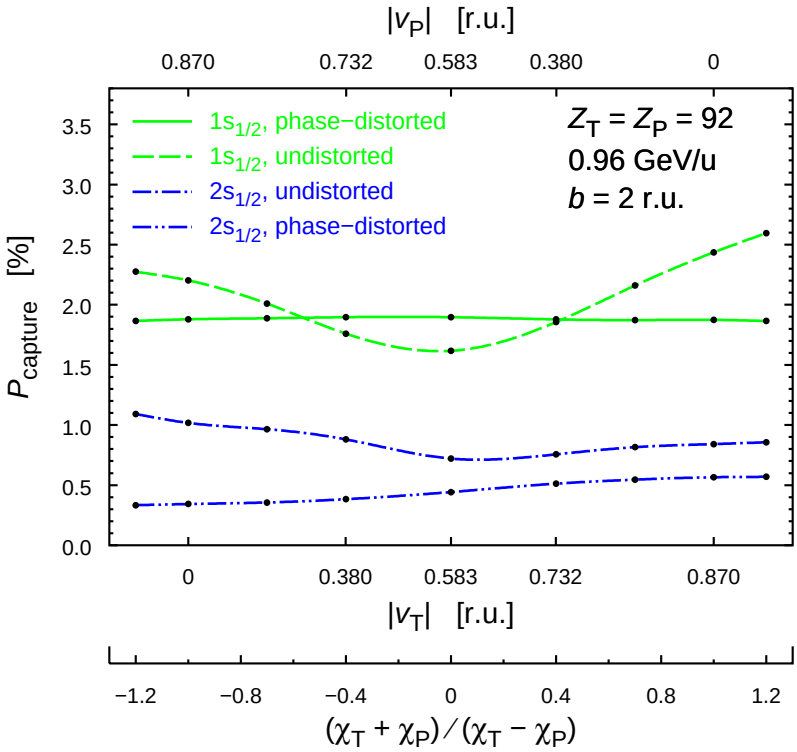

FIGURE 6.21. The frame dependence of the capture probability for the same collision parameters as in figure 6.11. The only difference to figure 6.11 is that the probabilities shown here have been computed with a basis of 68 basis functions, which comprises the 48 wave packets described in section 6.6.

using bases comprising bound states only, the results obtained with free-particle bases should be compared with the pure capture calculations. No such investigation exists in the literature.

Two different questions may be addressed. First, the influence of the free-particle basis functions on the calculated total cross section of electron capture may be investigated. Since ionisation probabilities are expected and, indeed, found to be much larger than capture probabilities, at least for the collision energies considered here, it could be that the omission of free-particle basis functions introduces a significant systematic error in the calculated capture cross sections. Second, it is interesting to ask, whether the addition of free-particle states to the coupled channel basis reduces the frame dependence of the capture probabilities. This has been conjectured in section 6.1.

In comparison to the pair creation process, the main contributions to electron capture cross sections come from larger impact parameters. The physical reason is that pair creation requires much stronger electromagnetic fields; in peripheral collisions, the peak energy density of the electromagnetic field of the nuclei increases as the impact parameter decreases [TEL87]. The calculations presented in the previous section had to be extended to impact parameters up to $b = 10\,\mathrm{r.u.}$ in order to obtain the full impact-parameter dependence of electron capture in calculations also employing free-particle states. For the results of this section, the basis described in

the previous section has been used and the same collision system and energy have been considered, namely $Z_A, Z_B = 92$ and $T = 0.96\,\mathrm{GeV/u}$.

6.7.1 Total capture cross section. In figure 6.7 weighted capture-probabilities are presented that have been obtained by coupled channel calculations in the rest frame of nucleus A. Two different initial conditions are shown in each plot. Several different bases have been used. The two diagrams at the top of figure 6.7 represent calculations using a pure bound-state basis. This data has appeared already in figure 6.10 and is replotted to allow for a convenient comparison. The other four plots show results from calculations with bases comprising free-particle states.

It has been found that ionisation probabilities in numerical calculations of this work, which make use of free-particle states, are approximately one order of magnitude *larger* than the capture probabilities shown here. Since ionisation is not accounted for in coupled channel calculations with bases comprised of bound states only, it is remarkable that the omission of free particle states does *not* have major effect on the capture cross section. It is seen that the addition of free-particle states slightly enhances the capture cross section in calculations with undistorted bases. The opposite behaviour is exhibited by the capture probabilities corresponding to phase-distorted bases. Note that the frame dependence of the capture probabilities has nearly vanished in the calculation with phase-distorted states which employs wave packets at both centres (plot at the bottom right of figure 6.10).

6.7.2 Frame dependence. For the impact parameter $b = 2\,\mathrm{r.u.}$ the total capture probability has been evaluated in various frames of reference, using the fully symmetrical basis described in the previous section, comprised of the ten lowest bound states and 24 stationary wave packets of each centre. The results are shown in figure 6.21. Analogous calculations using a pure bound-state basis have been presented in figure 6.11 on page 82. Comparing these two figures the reduced frame dependence due to the addition of free-particle states is clearly noticed in figure 6.21. The reduction of the frame dependence is very convincing for the calculation with phase-distorted basis functions, in particular if the $1s_{1/2}$ initial configuration is considered. Although a diminished frame dependence is present also for calculations with undistorted bases, it is less satisfactory, presumably reflecting that the coupled channel basis is still too small. Nevertheless, the present results demonstrate that the frame dependence of the numerically determined capture cross section is diminished by the adding of stationary wave packets to the coupled channel basis.